Temporal dynamics and environmental controls of carbon dioxide and methane fluxes measured by the eddy covariance method over a boreal river

Aki Vähä[1,2], Timo Vesala[1,3], Sofya Guseva[4], Anders Lindroth[5], Andreas Lorke[4], Sally MacIntyre[6,7], and Ivan Mammarella[1]

[1]Institute of Atmospheric and Earth System Research / Physics, University of Helsinki, Helsinki, Finland
[2]Tvärminne Zoological Station, University of Helsinki, Hanko, Finland
[3]Institute of Atmospheric and Earth System Research / Forest Sciences, University of Helsinki, Helsinki, Finland
[4]Institute for Environmental Sciences, RPTU Kaiserslautern-Landau, Landau, Germany
[5]Department of Physical Geography and Ecosystem Science, Lund University, Lund, Sweden
[6]Marine Science Institute, University of California, Santa Barbara, CA, USA
[7]Department of Ecology, Evolution, and Marine Biology, University of California, Santa Barbara, CA, USA
Correspondence: Aki Vähä (aki.vaha@helsinki.fi)

Abstract. Boreal rivers and streams are significant sources of carbon dioxide (CO_2) and methane (CH_4) to the atmosphere. Yet the controls and the magnitude of these emissions remain highly uncertain, as current estimates are mostly based on indirect and discrete flux measurements. In this study, we present and analyse the longest CO_2 and the first ever CH_4 flux dataset measured by the eddy covariance (EC) technique over a river. The field campaign (KITEX) was carried out during June–October 2018 over the River Kitinen, a large regulated river with a mean annual discharge of 103 m^3 s^{-1} located in northern Finland. The EC system was installed on a floating platform, where the river was 180 m wide and with a maximum depth of 7 m. The river was on average a source of CO_2 and CH_4 to the atmosphere. The mean CO_2 flux was 0.36 ± 0.31 µmol m^{-2} s^{-1} and the highest monthly flux occurred in July. The mean CH_4 flux was 3.8 ± 4.1 nmol m^{-2} s^{-1} and it was also highest in July. During midday hours in June, the river acted occasionally as a net CO_2 sink. In June–August, the nocturnal CO_2 flux was higher than the daytime flux. The CH_4 flux did not show any statistically significant diurnal variation. Results from a multiple regression analysis show that pattern of daily and weekly mean fluxes of CO_2 are largely explained by partial pressure of CO_2 in water (pCO_{2w}), photosynthetically active radiation (PAR), water flow velocity and wind speed. Water surface temperature and wind speed were found to be the main drivers of CH_4 fluxes.

1 Introduction

The global river network covers an area of about $624\,000$ km^2, which is approximately 15 % of the global inland water area (Raymond et al., 2013; Verpoorter et al., 2014). Despite their relatively small area, rivers and streams are significant sources of carbon (C) into the atmosphere in the form of carbon dioxide (CO_2) and methane (CH_4) (Raymond et al., 2013). Prior studies have estimated that $0.23 - 1.8$ Pg C yr^{-1} is released to the atmosphere from streams and rivers, mainly in the form of CO_2 (Cole et al., 2007; Aufdenkampe et al., 2011; Raymond et al., 2013; Regnier et al., 2013; Lauerwald et al., 2015; Drake et al.,

20 2018). As methane is a more potent greenhouse gas than carbon dioxide, its emission from rivers is of importance although the CH_4-C only accounts for a few percent of the total carbon flux (Cole et al., 2007). The most recent estimate of the outgassing magnitude for CO_2 was published by Li et al. (2021), who combined studies from 595 streams and rivers. Their global estimate for CO_2 annual emission is 1.8Pg C of which 72.3 % takes place in streams (Strahler orders 1–3) (Li et al., 2021). For CH_4, the most recent outgassing estimate is 27.9 Tg CH_4 per year (Rocher-Ros et al., 2023).

25 By far most of the river gas flux studies so far have been conducted using floating chambers that are point measurements in time and space (Bastviken et al., 2015; Lorke et al., 2015). In addition, the flux measurements and gas sampling tend to concentrate on daytime hours (Gómez-Gener et al., 2021) and mostly during calm and moderate wind speed with good weather conditions. Due to the magnitude of surface-layer turbulence and the processes producing or consuming CO_2 or CH_4 being dependent on location and time (Rocher-Ros et al., 2019; Gómez-Gener et al., 2021; Attermeyer et al., 2021), there

30 is inherently large spatial and temporal variability in the flux magnitude, which may not be captured with floating chambers (Hall and Ulseth, 2019). The eddy covariance (EC) method, which provides flux estimates for a certain averaging period and represents a much larger spatial domain than chambers, has been utilised over a river so far only once for CO_2 flux (Huotari et al., 2013), and never for CH_4. Therefore, due to the lack of continuous and long term flux timeseries, knowledge gaps exist in resolving the diurnal, seasonal and interannual variability of the air-water gas exchange and in the significance of different

35 physical and biogeochemical processes in rivers and streams of different sizes.

To address this gap, we conducted an experiment on the subarctic River Kitinen in northern Finland during June–October 2018 in the Kitinen Experiment (KITEX) campaign. The goal of the campaign was to measure and quantify the CO_2 and CH_4 fluxes (F_{CO_2} and F_{CH_4}, respectively) with an EC system on a floating platform as well as the physical forcings driving the fluxes. The River Kitinen is a regulated river and, as such, provides information on e.g., how the anthropogenic modification

40 of the flow affects the gas exchange.

The aims of this study are to provide four-month time series of both CO_2 and CH_4 fluxes and to quantify the response of the fluxes to different environmental drivers. In addition, we present the diurnal patterns of the gas fluxes, analyse their possible causes, and discuss to what extent the under-representation of flux temporal dynamics in existing database, largely based on discrete sampling, may bias estimates of CO_2 and CH_4 emissions from river systems. Finally, we propose a new approach to

45 minimize the effect of a limited fetch on the measured fluxes, advancing methodological approaches pertaining to the use of EC technique in relatively small inland water bodies.

2 Material and methods

2.1 Site description

The River Kitinen in northern Finland is 235 km long and has a catchment area of 7672 km^2 (Fig. 1a). The catchment area

50 consists mostly of managed boreal forest with Scots pine (Pinus sylvestris) and Norway spruce (Picea abies) as the main tree species, wetlands of which a large portion is drained, small streams and rivers, some low mountains and a few small settlements. Forests cover approximately 67 % and wetlands 25 % of the catchment. The soil in the catchment area consists mainly of sandy

moraine and peat. The catchment area is relatively flat, the height above sea level being 100–200 m in the south and 200–300

m in the north and exceeding 400 m only in a few places. Consequently, the mean slope of the river is just 0.5 m km^{-1}. The

55   River Kitinen is heavily regulated with altogether seven hydropower plants and corresponding reservoirs along its length. The

river is a tributary of the larger River Kemijoki.

    Kitinen's catchment area belongs to the subarctic climate zone (Köppen classification Dfc). The annual mean temperature

(related to the Finnish Meteorological institute's reference period 1991–2020) is $0.3°$C and the annual mean precipitation is

543 mm. Permafrost does not exist in the region. The vegetation growing period in the area normally lasts from mid-May until

60   late September. The river freezes every winter, usually in October–November and the ice breakup normally takes place in May.

In 2018, the breakup occurred in mid-May.

    The experiment site ($67.37°$ N, $26.62°$ E, 173 m above sea level) was located next to the Finnish Meteorological Institute's

research and weather station in Tähtelä (Figs. 1b–c), 5 km south of the town of Sodankylä. At the experiment location the

river is 180 m wide and forms a straight section extending approximately 600 m upstream and 1000 m downstream from the

65   site. The direction of the river at the site is roughly north-northwest–south-southeast and it flows towards the south. The mean

annual discharge, measured at the closest power plant downstream, is 103 m^3 s^{-1}. The maximum depth at the site is 7 m. The

river bed consists mainly of sand with some overlaying biological deposits. The River Kitinen's Strahler stream order at the

site is 5, based on hydrographical data that include headwater streams with a catchment area larger than 10 km^2.

    The closest hydropower plants to the site are located 11 km upstream and 11 km downstream. The water flow velocity at the

70   experiment site was almost completely controlled by the hydropower dam regulation downstream. Flow regulation in the river

followed a certain pattern where the flow would be small or completely halted during most nights (Guseva et al., 2021).

    The eddy covariance, meteorological and water flow measurements were conducted on a floating platform, located about 70

m from the eastern river bank, where the water depth was 4.5 m. The platform was 6 m × 3 m and was constructed of a marine

plywood deck on top of plastic pontoons. The deck was 0.5 m above the water surface. The platform was anchored with four

75   concrete blocks and held in its position with four anchor lines that each also had a large buoy attached, keeping the line tight.

The anchoring blocks had a mass of 200 kg and were placed 20–30 m away from the platform's corners. The anchoring made

the platform very stable and the motion of the platform was minimal. Electricity was provided to the platform by a power cable.

    The campaign lasted from 1 June until 17 October 2018. Eddy covariance measurements took place from 1 June to 2 October.

2.2 Eddy covariance measurements

80   The EC system measuring water–atmosphere turbulent fluxes was mounted on a mast on the southern side of the platform.

This installation consisted of an ultrasonic anemometer (uSonic-3 Scientific, METEK Meteorologische Messtechnik GmbH,

Elmshorn, Germany) for measuring the wind speed in three Cartesian coordinates u, v and w and the sonic temperature T_s, an

enclosed-path gas analyser (LI-7200RS, LI-COR Biosciences, Inc., Lincoln, Nebraska, USA) for measuring carbon dioxide and

water vapour mole fractions χ_{CO_2} and χ_{H_2O}, and a closed-path gas analyser (G1301-f, Picarro, Inc., Santa Clara, California,

85   USA) for measuring methane and water vapour mole fractions χ_{CH_4} and χ_{H_2O}. The centre of the sonic anemometer was 1.82

m above the water surface. The gas analyser sampling line inlets were placed 2 cm below the sonic anemometer and their
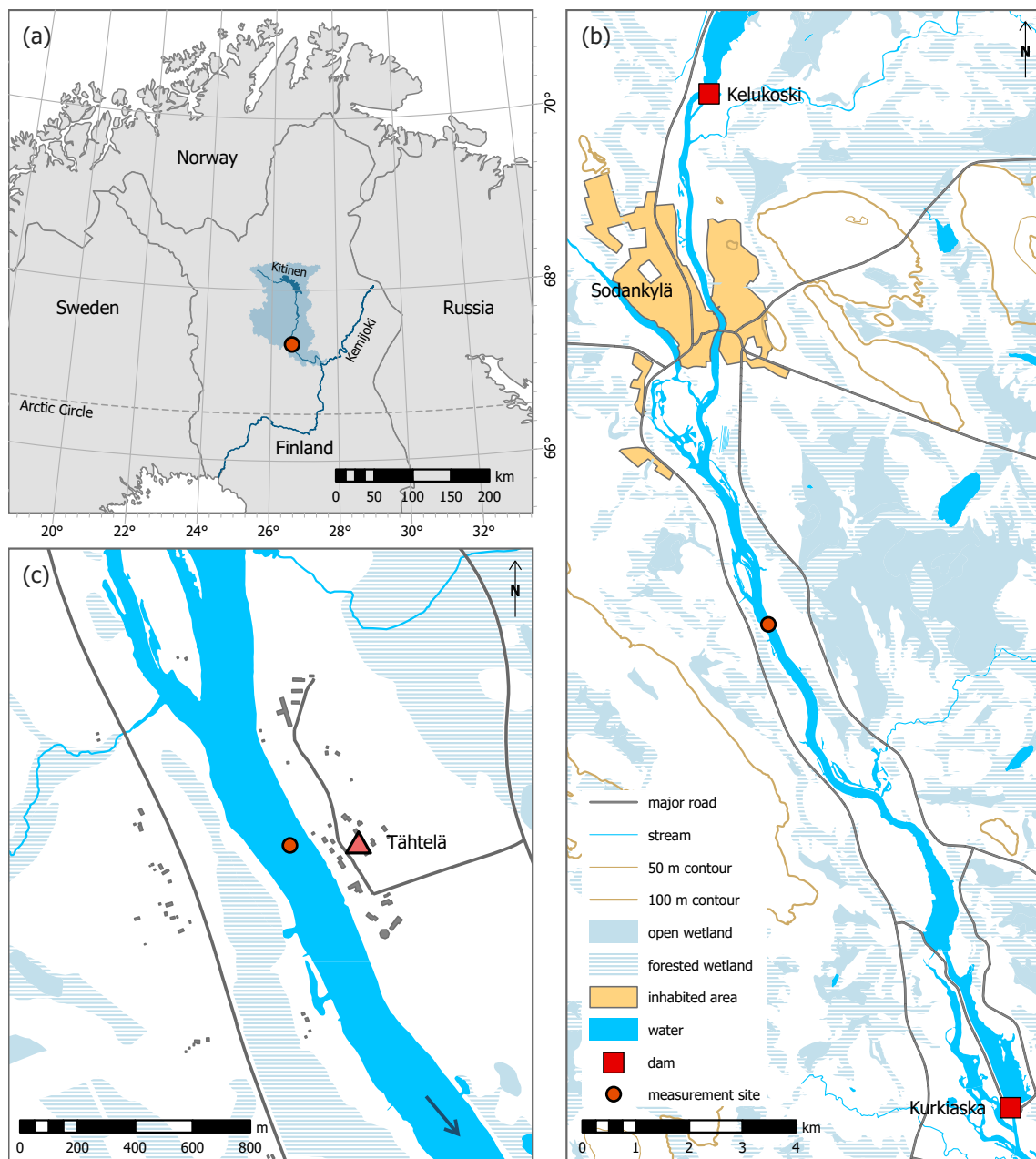
Figure 1. (a) Location of the River Kitinen (blue line) and its catchment area (light blue area) in northern Finland. The site of the experiment is marked with a red dot. The larger River Kemijoki is drawn with a dark blue line. (b) General area of the measurement site. Hydropower plants closest to the site are indicated with red squares. (c) Immediate surroundings of the experiment site. The arrow indicates the flow direction. The red triangle shows the location of the Tähtelä weather station. Buildings are marked with grey polygons. Map data sources: (a) naturalearthdata.com (base map); Finnish Environment Institute, 12/2020 (hydrographical data). (b–c) National Land Survey of Finland Topographic Database, 12/2020.

horizontal separation from the centre of the sonic anemometer was 3 cm. The inlets were equipped with rain guards and fine mesh filters. The LI-7200RS's sampling line was made of AISI 316 stainless steel. Its length was 1.0 m, it was 6.4 mm in outer and 4.4 mm in inner diameter, and it was heated at a constant rate of 6 W m^{-1}. The flow rate was 12 l min^{-1}. The G1301-f

90 sampling line was made of PTFE (teflon), it was 10 m in length, 6.4 mm in outer diameter, 4.4 mm in inner diameter and was heated at a constant rate of 9.5 W m^{-1}. The flow rate was 16 l min^{-1}. An inclinometer (DOG2 micro-electro-mechanical system, Measurement Specialties, Inc., Hampton, Virginia, USA) was used for measuring the pitch and roll of the platform.

The sampling rate of ultrasonic anemometer, gas analysers and the inclinometer was 10 Hz and were recorded on mini-computer by using an in-house data logging software.

95 A calibration system for LI-7200RS began operating on 29 August until the end of the campaign. The calibration consisted of driving 5 min of synthetic air with 0 ppm of CO_2 and 5 min of synthetic air with 450 ppm of CO_2 through the gas analyser once a day. Calibration was solved for both the offset and the span in the CO_2 mixing ratio. The offset was negligible. In contrast, there was 1.3 % span correction applied to the measured CO_2 mole fraction data. The G1301-f was not calibrated on field but instead the factory calibration was used.

2.3 Eddy covariance data processing

EC fluxes were calculated using the EddyUH software (Mammarella et al., 2016), following the state of art methodologies (Sabbatini et al., 2018; Nemitz et al., 2018). Rawdata were despiked based on the maximum difference allowed between two subsequent data points, according to the threshold values listed in Table 1. The dilution and spectroscopic correction (Chen et al., 2010) were applied point-by-point to the measured CH_4 mole fraction using the simultaneous H_2O mole fraction

105 measured in the sampling cell of the Picarro analyser. The LI7200RS internally corrects the water-induced density effect and gives as an output the dry mole fraction of CO_2. No density corrections were therefore needed for CO_2 (Burba et al., 2012). Although operated, the inclinometer data were not used for correcting the wind velocity components. It was checked from cospectra of $\overline{u'w'}$ and $\overline{v'w'}$ that the differences between the inclinometer-corrected and uncorrected velocities were only random. Instead, the inclinometer data was used in screening out the occasions when the movement of the platform was too

110 big, i.e. when there were persons on the platform. A crosswind correction of sonic temperature was applied according to Liu et al. (2001). Additionally, a double coordinate rotation was applied to the sonic anemometer data by forcing the mean values of lateral (v) and vertical (w) velocity components of wind to zero.

Gas fluxes were calculated from the covariance between the vertical wind speed w and the gas dry mole fraction χ, multiplied by the molar density of air ρ_a, as

115 $$F_\chi = \rho_a \overline{w'\chi'}, \tag{1}$$

where the overbar denotes the time average and the prime the deviation from the mean. An averaging time of 30 minutes was used. The time series were linearly detrended so that the turbulent fluctuation in equation (1) was defined as the deviation from the linear trend. Per definition, a positive flux indicates an upward flux (from the surface to the atmosphere).

Table 1. Threshold values for detecting spikes in different variables.

Variable	Threshold
u, v	10 m s^{-1}
w	7 m s^{-1}
T_s	10°C
χ_{CO_2}	100 ppm
χ_{H_2O} (Li-7200RS)	50 mmol mol^{-1}
χ_{CH_4}	100 ppb
χ_{H_2O} (G1301-f)	50 mmol mol^{-1}

Before calculating the covariance, the time lag between w and χ was removed. The time lag was determined by finding the
120 maximum difference of the cross-covariance of w and χ to a line between covariance values at the lag window limits within a
given lag window (Aubinet et al., 2000). Due to the low signal-to-noise ratio and in order to reduce the possible mirror effect
of the fluxes around zero (Kohonen et al., 2020), a constant lag of 0.34 s was used for CO_2 and 7.0 s for CH_4. These values
were calculated as the mean values of estimated time lag distribution. For H_2O, a relative humidity (RH) dependent time lag,
varying from 0.30 s to 1.8 s, was used in order to account for the H_2O sorption in the sample line.

125 Fluxes were corrected for both low and high frequency attenuation. The actual unattenuated flux F is calculated from the
measured flux F_χ as

$$F = \frac{F_\chi}{F_\text{a}}, \tag{2}$$

where F_a is the flux attenuation. It is defined as the integral of a model cospectrum $C_\text{model}(f)$ and the total transfer function
TF, normalised by the model cospectrum:

$$130 \quad F_\text{a} = \int_0^\infty C_\text{model}(f)\text{TF}(f)\text{d}f \bigg/ \int_0^\infty C_\text{model}(f)\text{d}f. \tag{3}$$

TF is a product of the high- and low-frequency transfer functions that describe the attenuation at different frequencies (f).

The low-frequency flux attenuation stems from the linear detrending of the original timeseries (Rannik and Vesala, 1999).
The theoretical transfer function in this case is

$$\text{TF}_\text{LF} = 1 - \frac{\sin^2{(\pi f T_\text{av})}}{(\pi f T_\text{av})^2} - 3\frac{[\sin{(\pi f T_\text{av})} - \pi f T_\text{av}\cos{(\pi f T_\text{av})}]^2}{(\pi f T_\text{av})^4}, \tag{4}$$

135 where T_av is the averaging time. The high-frequency correction of fluxes was solved using an experimental transfer function
(Aubinet et al., 2000). It is assumed that the temperature cospectrum $C_{w\theta}$ is unattenuated and therefore used as reference
cospectrum. The measured transfer function is then

$$\text{TF}_\text{meas} = \frac{N_\chi C_{w\chi,\text{meas}}}{N_\theta C_{w\theta}}, \tag{5}$$

where N_χ and N_θ are normalisation factors equal to the covariances $\overline{w'\chi'}$ and $\overline{w'\theta'}$, respectively. The following functional

140 form was then fitted to the measured values of Eq. (5)

$$\mathrm{TF_{HF}} = \frac{1}{(1 + 2\pi f \tau)^2},\tag{6}$$

where τ is the response time. Similarly as with the lag time determination, the response time was not affected by sorption effect in the case of CO_2 and CH_4 fluxes and a constant response time $\tau = 0.185$ s for CO_2 and $\tau = 0.2$ s for CH_4 could be used. In contrast, τ for H_2O is relative humidity-dependent (Mammarella et al., 2009). In this case, τ was determined by dividing the

145 measured cospectra into six RH classes and calculating the bin mean. Then, a curve of the form

$$\tau_{H_2O} = b_1 + b_2 (RH/100)^{b_3}\tag{7}$$

with $b_1 = -0.057$, $b_2 = 0.79$, $b_3 = 1.6$ was fitted to the averaged data.

  The model cospectrum in equation (3) was determined by fitting the function proposed by Kristensen et al. (1997) to the measured normalised temperature cospectrum $C_{w\theta}$

150 $$C_{\mathrm{model}}(n) = \frac{a \cdot \frac{2\pi}{z} n}{\left[1 + (2\pi n L)^{2\mu}\right]^{7/(6\mu)}},\tag{8}$$

where $n = zf/U$ is the normalised frequency, z is the measurement height and U is the mean wind speed. The fit parameters were $a = 6.78$ m, $L = 1.35$ and $\mu = 0.32$ for unstable cases and $a = 57.00$ m, $L = 1.84$ and $\mu = 0.17$ for stable cases.

  The following criteria were used in the post-processing quality control of the fluxes: skewness SK and kurtosis KU of both w and the dry mole fraction χ of the gas in question ($-2 < SK < 2$, $1 < KU < 8$) (Vickers and Mahrt, 1997), flux stationarity

155 ($FST \leq 1$) (Foken and Wichura, 1996), the number of spikes (≤ 1800 in a 30-minute averaging period), the wind direction, and occasions when the platform swayed too much, most often due to persons on the platform. As suggested by Erkkilä et al. (2018), additional filtering was done based on threshold values of standard deviation of carbon dioxide ($\sigma_{\chi_{CO_2}}$) and methane $\sigma_{\chi_{CH_4}}$ mixing ratios. The criteria removed 30 min flux values when $\sigma_{\chi_{CO_2}} < 1$ppm and $\sigma_{\chi_{CH_4}} < 0.013$ppm.

  In order to find acceptable wind sectors, the flux footprint model by Kljun et al. (2015) was used. Parameters for the foot-

160 print calculation were the friction velocity u_*, standard deviation of lateral wind velocity σ_v, wind direction and the calculated Obukhov length L_{MO}. We assume a constant boundary layer height $h_{BL} = 1000$ m and roughness length $z_0 = 0.01$ m. The resulting footprint climatology, depicted in Fig. 2, is roughly oval-shaped with the long axis approximately along the river. Estimates for the footprint are generally not applicable with changing roughness, therefore, the river bank directions are excluded from the analysis. The longest distance to the 90 % footprint line at the southern side over the river is 177 m. Sectors where the

165 river bank was further than 177 m from the platform were accepted. The two sectors are 123°–181° and 285°–355°.

  However, there were numerous cases where the average 30-minute wind direction was seemingly from an accepted sector, but the instantaneous wind direction was at least partly from a rejected sector. In some cases, this had a considerable effect on the measured concentration and flux values, as the surrounding land was a source or sink of carbon dioxide, depending on the time of the day, and a source of methane. In addition, the magnitude of these sources or sinks can be larger than in the river. An
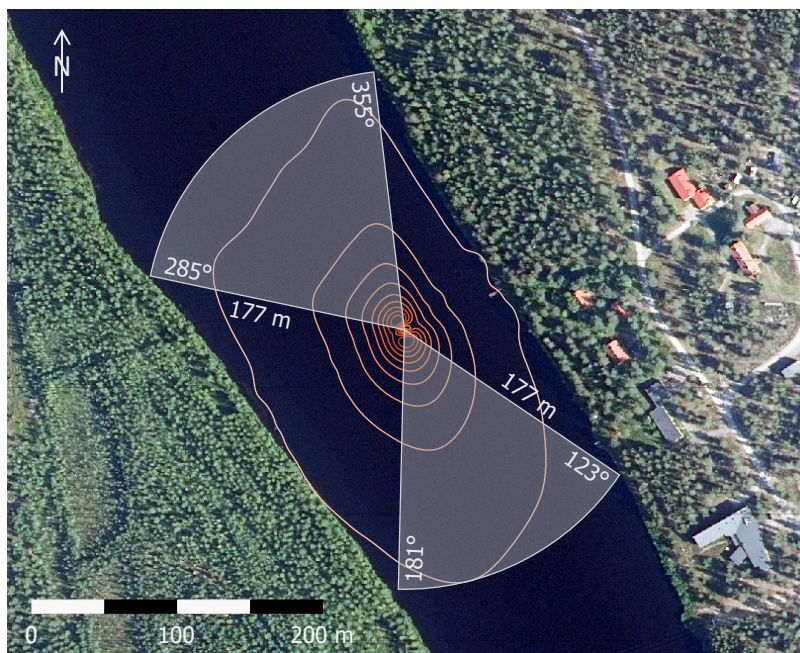
Figure 2. Flux footprint climatology. The curves show the footprint percentiles at 10 % intervals, starting from the outermost 90 % footprint. The grey sectors are the accepted wind directions. Image contains data from the National Land Survey of Finland Topographic Database, 12/2020.

170   example of such a case is shown in Fig. A1 when an air mass from the land caused an abrupt increase in the CO_2 mixing ratio and decrease in temperature after 23:53 UTC. In this case, the stationarity value of the CO_2 flux was 0.35, i.e. it passed the criterium FST < 1. To mitigate this effect, the following approach was used. Fluxes were calculated for 5-minute subintervals. If the mean wind direction fell within the accepted sectors in all of the six subintervals, the corresponding 30-minute flux value was retained. If more than one but less than six subintervals fell within the accepted sectors, their average was used as the value

175   for the flux for that 30-minute record. The record with one or none accepted 5-minute subintervals were discarded. This method still potentially leaves intermittent periods of wind from land for less than five minutes in the accepted data, but reduces their amount and their contribution to the final fluxes. Evidently, when the average of the 5-minute fluxes was used, it is a better approximation of the river surface exchange than the corresponding 30-minute flux as the difference between the 30-minute fluxes and the averaged 5-minute fluxes reduces with an increasing number of averaged 5-minute intervals (Fig. A2).

180   After the flux calculation and the raw data quality control, there were altogether 4534 30-minute flux data records. Table 2 summarises all flux quality control criteria and how much of the original 30-minute data retained after applying the criteria. In total, 43.9 % of the original F_{CO_2} records and 38.9 % of the original F_{CH_4} records remained after the quality control. Wind direction and standard deviation of gas mixing ratios were the most prominent criteria and removed approximately one fourth and one fifth of all the data, respectively. Most of the applied criteria overlapped with each other.

Table 2. The applied post-processing quality criteria and the amount of data they retain. SK: skewness, KU: kurtosis, WD: wind direction, FST: flux stationarity.

Criterium	Data records retained	% of all data
$SK(w) \in (-2,2)$	4534	100
$KU(w) \in (1,8)$	4468	98.5
WD	3265	72.0
too large movement of platform	4404	97.1
$SK(\chi_{CO_2}) \in (-2,2)$	4230	93.3
$KU(\chi_{CO_2}) \in (1,8)$	4111	90.7
$FST(F_{CO_2}) < 1$	3921	86.5
$SK(\chi_{CH_4}) \in (-2,2)$	3892	85.8
$KU(\chi_{CH_4}) \in (1,8)$	3597	79.3
$FST(F_{CH_4}) < 1$	3668	80.9
$\sigma\chi_{CO_2} < 1$ ppm	3559	78.5
$\sigma\chi_{CH_4} < 0.013$ ppm	3674	81.0
$total(F_{CO_2})$	1904	41.9
$total(F_{CH_4})$	1686	37.2

2.4 Ancillary measurements and data processing

Ambient air temperature (T_a) and relative humidity were measured with a Rotronic HC2-S3C03 probe (Rotronic AG, Bassersdorf, Germany), mounted inside a Young model 41003 (R. M. Young Company, Traverse City, Michigan, USA) multi-plate radiation shield on the platform's north-eastern corner. T_a and RH were available only after 15th of June. Before that, the sonic temperature and humidity calculated from χ_{H_2O}, measured with the LI-7200RS, were used instead. Atmospheric pressure p_{atm} and precipitation were measured at the Tähtelä weather station. Photosynthetically active radiation (PAR) in water was measured with two LI-192 sensors (LI-COR Biosciences, Inc., Lincoln, Nebraska, USA). The sensors were hanging from wires at 0.3 m and 1.0 m depths on a beam on the southern side of the platform. In the analysis, we used the sensor at 0.3 m.

Measurements of water side CO_2 partial pressure (pCO_2) were done by using an off-axis integrated cavity output spectrometer (Ultraportable Greenhouse Gas Analyzer – UGGA, Los Gatos Research, Inc., Santa Clara, California, USA) that was connected to the headspace of an equilibrator consisting of a floating Plexiglas chamber ($130 \times 500 \times 500$ mm) sticking about

50 mm into the water, leaving a headspace volume of about 20 l. The air in the headspace was circulated through the UGGA in a closed loop where the intake tube was fitted with a membrane (Accurel Polypropylene Capillary Membrane, Membrana GmbH, Germany) that prevented water from entering the UGGA. In order to increase the response time of the equilibrium concentration, a diffuser was placed in the water about 30 mm below the surface just beneath the chamber. The diffuser consisted of

200 a disc covered by a membrane with a large number of small holes. An external pump forced the air from the headspace through the diffuser at a rate of $2.5 \, \mathrm{l \, min^{-1}}$. A laboratory test showed that the time response of the system was about 40 minutes for 95 % change in concentration. The UGGA was connected to the equilibrator during 5 minutes every 20 minutes. The first 2 minutes after connection was skipped to allow the gas analyzer to adapt to the new condition (ambient air concentrations at 0.40 m and 2.40 m above the water surface were also monitored with the same system) allowing 3 minutes for averaging. The

205 UGGA was calibrated against reference gases (562–1188 ppm CO_2) with a specified accuracy of 2 %.

A water temperature chain was set up 100 m upstream of the platform. It consisted of five temperature loggers of the type RBR Solo (RBR Ltd. Ottawa, Ontario, Canada). The loggers were placed on a taut line mooring at depths of 0.35 m, 1.35 m, 2.35 m, 3.35 m and 4.35 m (6 June to 17 June) and 0.07 m, 1.05 m, 2.05 m, 3.05 m and 4.05 m (17 June onwards). The topmost measurement was used as the surface temperature. The water flow velocity was measured with a acoustic Doppler velocimeter

210 (Nortek Vector, Nortek AS, Rud, Norway) which was installed on a beam on the north-western corner of the platform, facing down (Guseva et al., 2021). The depth of the measurements was 0.4 m below the surface.

Spikes in ancillary data were identified with a MATLAB Hampel filter. The filter uses a moving window and identifies outliers with a standard deviation criterium. The filter parameters were hand-tuned for each variable. Spikes were replaced with linearly interpolated values.

215 ## 2.5 Multiple regression analysis

To study the drivers of the gas exchange, multiple linear regression between the fluxes and their possible drivers were tested. The driving variables were T_{surf}, PAR, wind speed (U), water flow speed (U_{w}), pCO_2 and precipitation (prec). All fluxes and environmental variables were distributed normally at a 95 % confidence level, thus making it possible to use regression models. Regressions were calculated on 24-hour and seven-day timescales, chosen to average diel and synoptic variations. Averages

220 were accepted when the data coverage was more than 30 %. Outliers in the averages were removed before calculating the regression models. The model results were ranked by the adjusted coefficient of determination R^2_{adj}. The adjusted R^2 was used instead of the ordinary R^2 to account for the artificial inflation of R^2 when more variables are added into a model.

Due to intercorrelation among the driving variables themselves, similar multiple regression calculations were conducted also for pCO_2 with water temperature, PAR, precipitation, wind speed and water flow speed as the driving variables.

3   Results

3.1   Environmental conditions

The 30-minute average air temperature rose from 10–20 °C at the beginning of the campaign to 30 °C in early August and then fell slightly below the freezing point towards the end of the campaign (Fig. 3a). The river surface temperature was 10 °C at the start of the campaign, reached its maximum value of 21.9 °C in the beginning of August and then fell close to the freezing point towards the end of the campaign (Fig. 3a), following closely the seasonal variation of air temperature. The water temperature difference between the river surface and the bottom was less than 2.2 °C at any time during the campaign (Fig. 3b). Stratification, defined as when the temperature difference between surface and bottom exceeded 0.05 °C, occurred when the flow was reduced, during 38 % of the campaign (Guseva et al., 2021).

The surface water at the platform was constantly supersaturated with CO_2 with respect to the atmosphere (Fig. 3c). The CO_2 partial pressure in the water $p_{CO_2,w}$ varied between 550 and 1323 ppm, the lowest values occurring in June and the highest in July. The daily variation of $p_{CO_2,w}$ ranged from 5 to 225 ppm.

The monthly precipitation was 43.7 mm in June (only the latter part of the month is shown), 61.4 mm in July, 75.9 mm in August and 78.5 mm in September-October (Fig. 3d). These correspond to approximately 25 % less than the average precipitation in June and July and about 40 % and 50 % more than average in August and September, respectively. In July, there was one heavy rain event that brought 41.5 mm of precipitation during one day.

The 30-minute mean wind speed varied between 0 and 8 m s^{-1} during the campaign months (Fig. 3e). The wind speed had both diurnal and synoptic variations and was largely channeled along the river (Fig. 4). The water flow speed varied from 0 to 0.33 m s^{-1} (Fig. 3f), showing as well a diel pattern due to the downstream dam operation (Guseva et al., 2021). Finally, underwater PAR measurements show expected diurnal and seasonal variations (Fig. 3g), with largest daytime values recorded in July (760 µmol m^{-2} s^{-1}) and the lowest at the end of the field campaign in September (60 µmol m^{-2} s^{-1}).

3.2 CO_2 and CH_4 fluxes

The quality-controlled 30 minute fluxes of CO_2 and CH_4 as well as their daily averaged values are shown in Fig. 5. Both F_{CO_2} and F_{CH_4} had a moderate seasonal variability showing higher fluxes in July and August. The monthly mean F_{CO_2} (standard deviation) was 0.19 (SD 0.31) in June, 0.34 (SD 0.32) in July, 0.44 (SD 0.32) in August and 0.41 (SD 0.24) µmol m^{-2} s^{-1} in September. The mean F_{CO_2} during the entire campaign was 0.36 (SD 0.31) µmol m^{-2} s^{-1}. The monthly mean fluxes are presented in Table 3.

The variability of F_{CO_2} was larger at nighttime compared to daytime during all months (Fig. 6, left panel). Performing a two-sample t test on F_{CO_2} during day- and nighttime (09:00–15:00 and 21:00–03:00 local time, respectively) in different months, there is also a statistically significant difference ($p < 0.05$) between the daytime and nighttime fluxes during June, July and August. In other words, during those months there was diurnal variation in the fluxes, the nighttime fluxes being higher. In September however, such variation did not exist. The mean nighttime F_{CO_2} (0.25 µmol m^{-2} s^{-1}) in June–September was
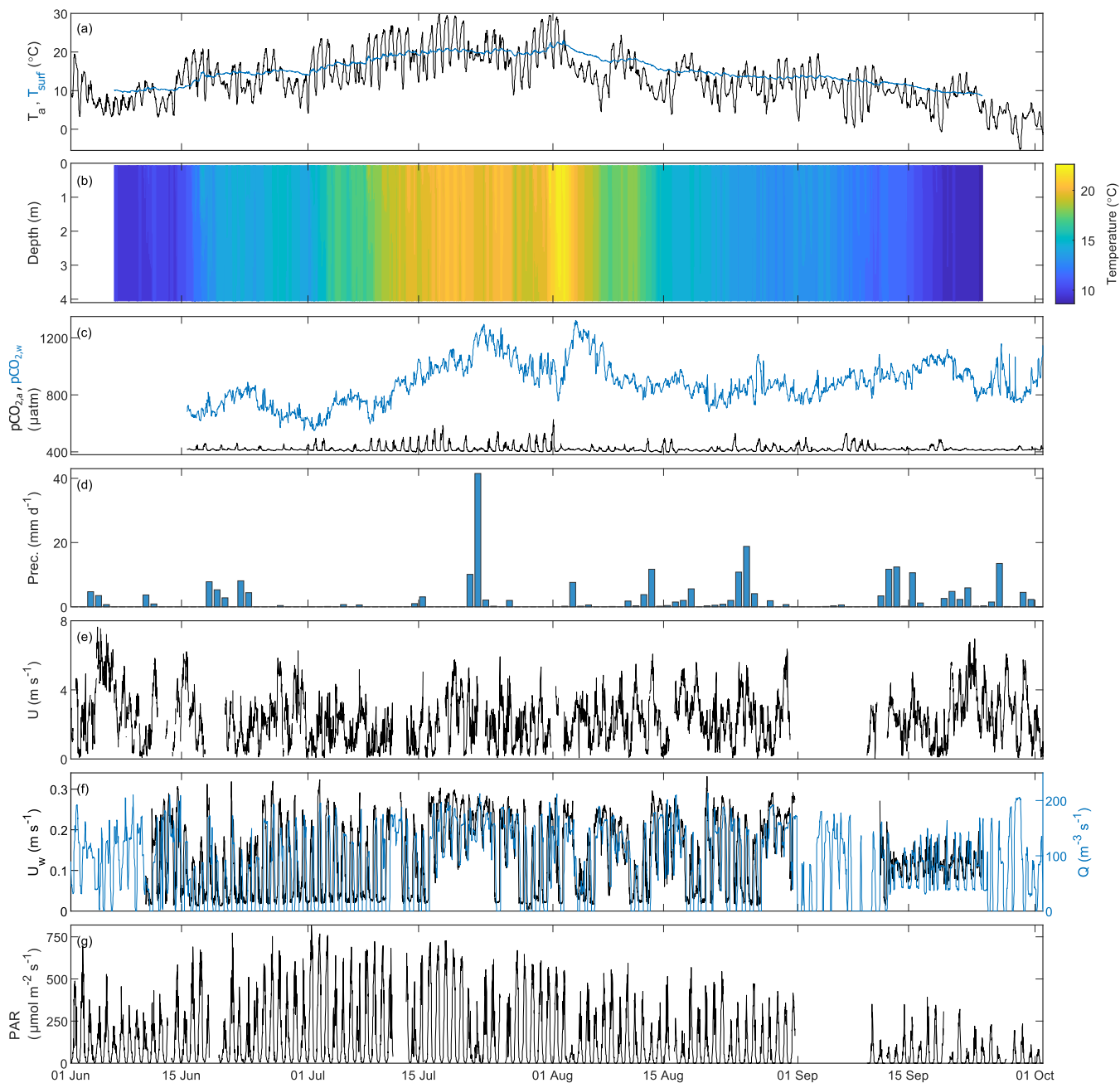
Figure 3. Environmental conditions during the campaign. The variables are shown as 30-minute average values, except for the precipitation data, which are shown as daily values. (a) Air temperature 2 m above river surface T_a (black) and water surface temperature T_{surf} (blue). (b) Contours of water temperature. (c) Atmospheric CO_2 partial pressure $p_{CO_2,a}$ (black) measured 0.4 m above the water surface and surface water CO_2 partial pressure $p_{CO_2,w}$ (blue). (d) Daily precipitation. (e) Wind speed U. (f) Water flow speed U_w (left, black) and discharge Q (right, blue). (g) Photosynthetically active radiation (PAR) at 0.30 m depth. Discharge was measured 11 km downstream. Precipitation was measured at the Tähtelä weather station.
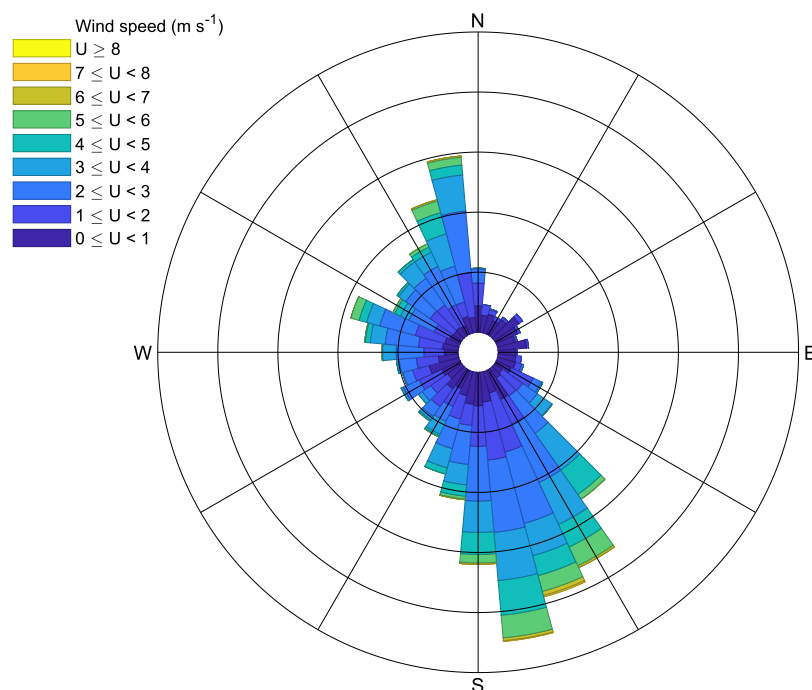
Figure 4. Wind climatology during the campaign.

220 % of the mean daytime F_{CO_2} (0.55 µmol m^{-2} s^{-1}). The day–night difference in F_{CO_2} was significant when observing the entire campaign's duration. Table 3 also contains the day- and nighttime mean fluxes.

The monthly mean F_{CH_4} (standard deviation) was 2.7 (SD 2.4) (June), 4.8 (SD 3.9) (July), 4.3 (SD 5.1) (August) and 3.3 (SD 4.1) nmol m^{-2} s^{-1} (September). The mean F_{CH_4} during the campaign was 3.8 (SD 4.1) nmol m^{-2} s^{-1}. Contrary to F_{CO_2}, there was no statistically significant diurnal variation in F_{CH_4} during any month of the campaign (Fig. 6, right panel). However, similarly as for F_{CO_2}, the day–night difference during the entire campaign's duration was significant but the daytime CH$_4$ fluxes were higher than during night. The measured nighttime F_{CH_4} (3.3 nmol m^{-2} s^{-1}) in June–September was 80 % of the daytime flux (4.1 nmol m^{-2} s^{-1}).

There was a period of relatively high fluxes on 19–25 July. The daily mean CO$_2$ fluxes reached 0.55–0.7 µmol m^{-2} s^{-1} and CH$_4$ fluxes 7–12 nmol m^{-2} s^{-1}. This period coincided with the discharge being constantly kept above 100 m^{3}s^{-1} and with the daily average winds being higher than during other times in July.

3.3 Relationship between the fluxes and environmental drivers

All possible combinations of the driving variables were tested, but here we present the five best models in each case. The models shown are statistically significant at a 95 % confidence level. There was intercorrelation between almost all driving variables, but the coefficient of determination was mostly low.

$F_{\mathrm{CO_2}}$ (μmol m^{-2} s^{-1})					
	June	July	August	September	June–September
Total	0.19 ± 0.31	0.34 ± 0.32	0.44 ± 0.32	0.41 ± 0.24	0.36 ± 0.31
Day	0.00 ± 0.34	0.31 ± 0.32	0.24 ± 0.28	0.37 ± 0.23	0.25 ± 0.32
Night	0.48 ± 0.18	0.70 ± 0.34	0.72 ± 0.31	0.41 ± 0.23	0.55 ± 0.29
Day–night difference	yes	yes	yes	no	yes
$F_{\mathrm{CH_4}}$ (nmol m^{-2} s^{-1})					
	June	July	August	September	June–September
Total	2.7 ± 2.4	4.8 ± 3.9	4.3 ± 5.1	3.3 ± 4.1	3.8 ± 4.1
Day	3.2 ± 2.4	4.8 ± 3.6	4.7 ± 6.0	3.5 ± 4.7	4.1 ± 4.4
Night	2.5 ± 2.1	5.1 ± 3.6	4.0 ± 3.7	2.9 ± 3.6	3.3 ± 3.3
Day–night difference	no	no	no	no	yes

Table 3. Mean fluxes and their standard deviation in each month during the campaign and the overall mean fluxes. The mean fluxes and the standard deviation are also shown for day- and nighttime during each month. The day–night difference indicates whether there was a statistically significant difference in the fluxes between day and night.

The best models for $p\mathrm{CO_{2w}}$ are similar at daily and weekly timescales (Table 4). $p\mathrm{CO_{2w}}$ was mainly driven by T_{surf}, PAR and U_{w}. Some of best daily models include U. The response to T_{surf} and U_{w} was positive, while it was negative for PAR. An exception is the negative response to U_{w} in the best weekly model. This model also includes precipitation as a driver. The
275 adjusted coefficient of determination R^2_{adj} was 0.407 and 0.516 for the best daily and best weekly model, respectively.

The best regression model for the $\mathrm{CO_2}$ fluxes on a daily timescale contains $p\mathrm{CO_{2w}}$, PAR and U_{w} and U (Table 5). The coefficient between these variables and $F_{\mathrm{CO_2}}$ is positive except for PAR. Two models with the best second R^2_{adj} value includes also precipitation or T_{surf} as additional explanatory variables. The models respond positively to both precipitation and T_{surf}. The explanatory variables $p\mathrm{CO_{2w}}$,U_{w} and U appear in all of the five best models. The best model on a weekly timescale contains
280 most of the selected environmental parameters, except PAR, which appears in the last three best models with a negative response. Almost all models also contain precipitation. R^2_{adj} was 0.621 for the best daily model and 0.928 for the best weekly model. The models' response to $p\mathrm{CO_{2w}}$, U_{w} and U was positive at both weekly and daily timescales, while the response to PAR was always negative. The models had variables response to T_{surf} and precipitation.

The best models for $\mathrm{CH_4}$ fluxes on both daily and weekly timescales all contain T_{surf} and the fluxes' response to T_{surf} is
285 positive. The best models on a daily scale additionally contain U. On the weekly scale, most of the best models also include PAR. R^2_{adj} is only 0.19–0.22 on a daily timescale due to the large scatter in the data. On a weekly scale, R^2_{adj} is high because the amount of weekly data was small.
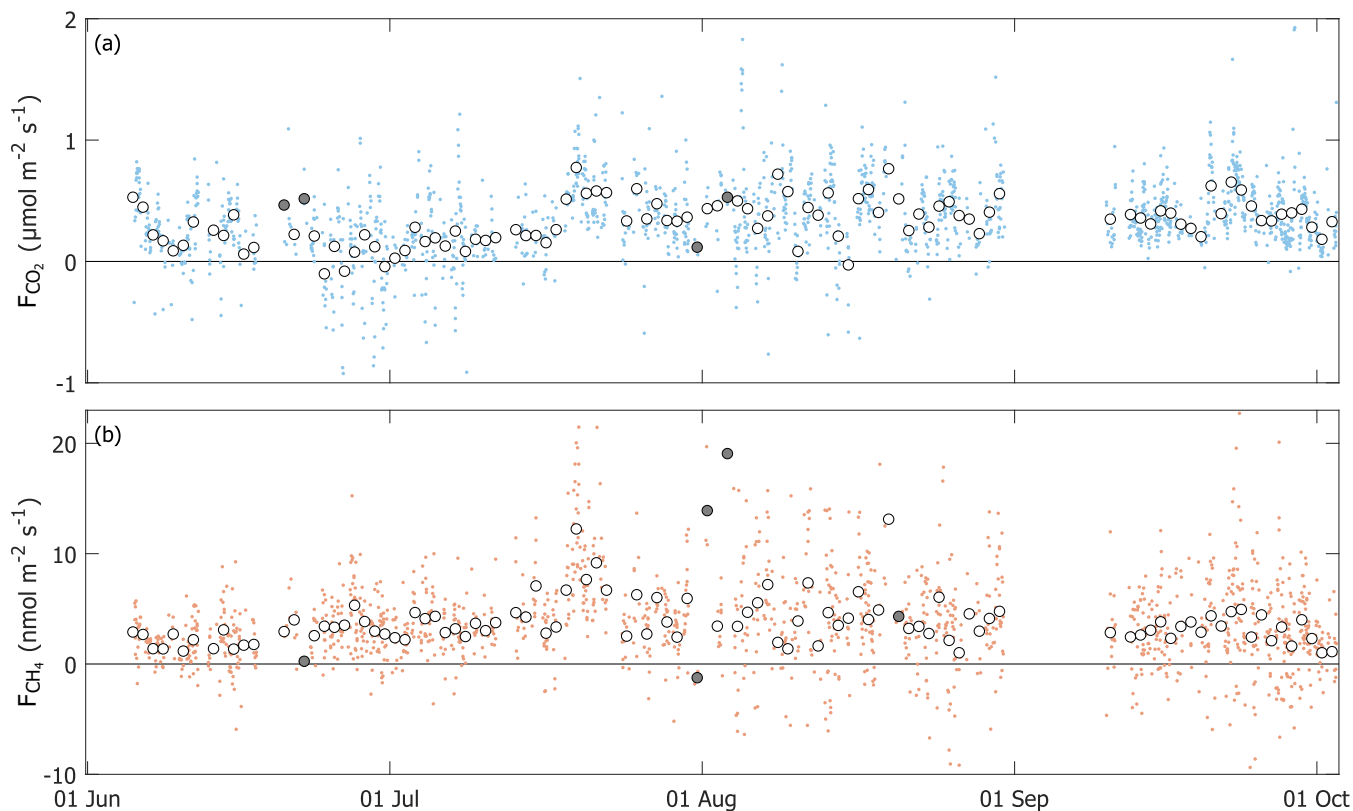
Figure 5. Time series of the CO_2 (top) and CH_4 flux (bottom). The dots indicate the 30-minute values and the circles indicate the daily averages. Fluxes are quality-controlled. The daily fluxes are drawn with a dark circle if the day contained only three or less 30-minute fluxes.

4 Discussion

4.1 Challenges of EC flux measurements over river

290 The EC technique is widely used for continuous and long-term monitoring of energy and gas exchange between land ecosystems (forest, wetland, arable land, grassland) and atmosphere (Baldocchi, 2003). The method has been applied only recently to inland aquatic ecosystems, and at the moment there is no comprehensive network of long-term EC sites covering different latitude and climatic zones, and water bodies characteristics. Most of the previous EC studies over inland water bodies have focused on lakes and on their water-atmosphere energy exchange, while only few studies have reported direct EC fluxes of

295 CO_2 and CH_4 over lakes (Mammarella et al., 2015; Czikowsky et al., 2018; Eugster et al., 2020; Golub et al., 2023). So far, only one study has reported CO_2 fluxes measured by EC technique over river (Huotari et al., 2013). While land-based EC flux measurements and data processing chains are well established (Sabbatini et al., 2018; Nemitz et al., 2018), standard EC data processing steps are not always applicable for measurements over inland water bodies. Fluxes are often smaller in magnitude than those typically found over land and the reduced turbulent mixing over a smooth water surface may lead to further lim-
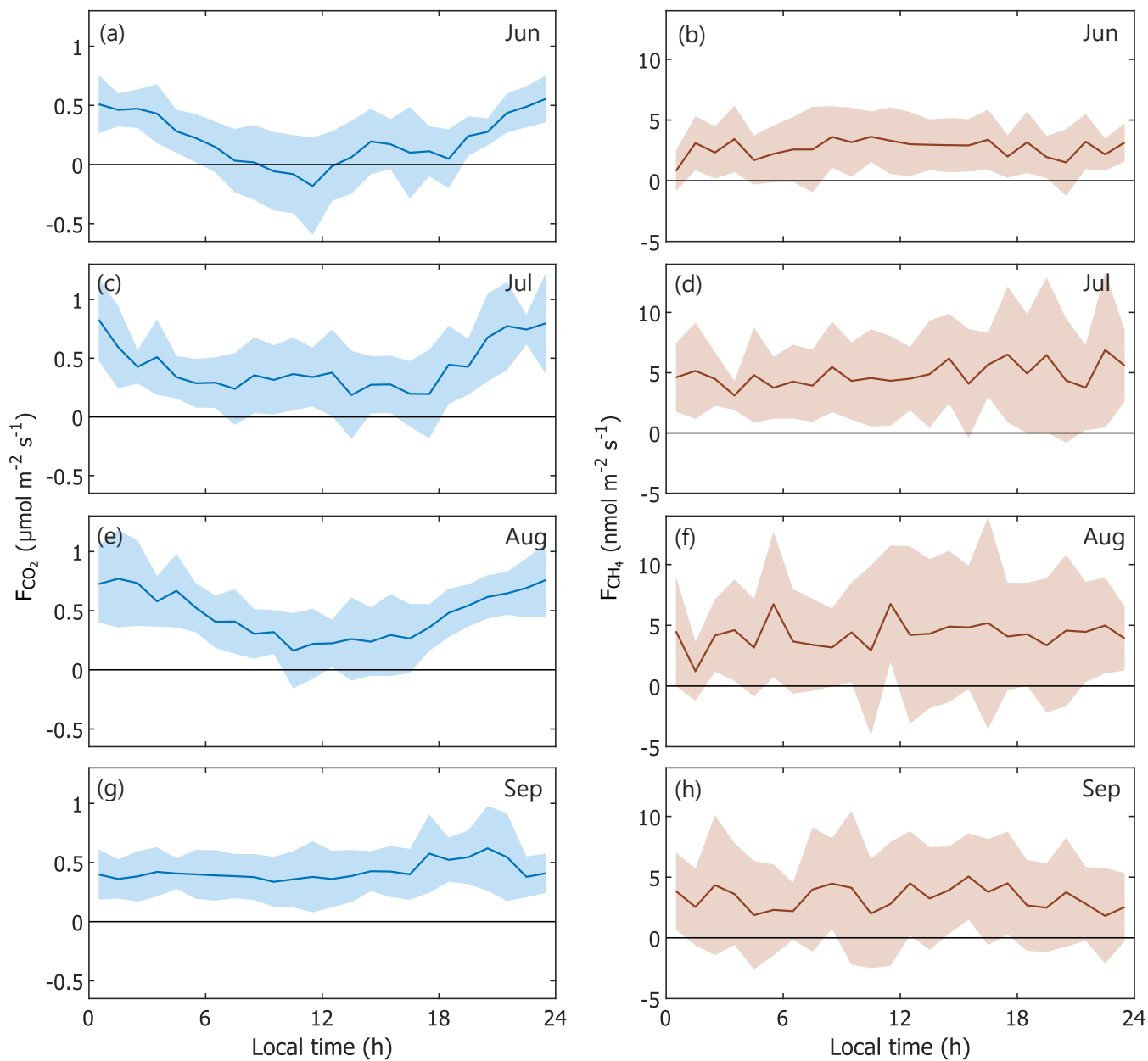
Figure 6. Diurnal variation of of CO_2 flux (a, c, e, g) and CH_4 flux (b, d, f, h) in different months, averaged in 1-hour bins. The line and the shaded area indicate the mean flux and its standard deviation.

Table 4. Multivariate linear regression models between the partial pressure of CO_2 in water (pCO_{2w}, [μatm]) and surface temperature (T_{surf}, [°C]), photosynthetically active radiation (PAR, [μmol m^{-2} s^{-1}]), wind speed (U, [m s^{-1}]), precipitation (prec, [mm d^{-1}]) and water flow speed (U_w, [m s^{-1}]) that give the highest value of R^2_{adj} at time scales (averaging periods) of 24 hours and 7 days. The Wilkinson notation is used in describing the combination of the variables. In the model formula, the unit of the intersection is μatm and the units of the variables' multipliers are μatm/[unit of variable]. Only statistically significant models are shown.

Combination	Formula	R^2_{adj}
24 h		
$T_{surf} + PAR + U_w$	$563 + 25.7\,T_{surf} - 1.18\,PAR + 586\,U_w$	0.407
$T_{surf} + PAR + prec + U_w$	$561 + 25.4\,T_{surf} - 1.14\,PAR + 49.3\,prec + 582\,U_w$	0.402
$T_{surf} + PAR + U_w + U$	$77 + 25.5\,T_{surf} - 1.19\,PAR + 561\,U_w - 2.62\,U$	0.392
$T_{surf} + PAR + prec + U_w + U$	$575 + 25.1\,T_{surf} - 1.14\,PAR + 59.8\,prec + 556\,U_w - 2.86\,U$	0.386
$T_{surf} + PAR + U$	$754 + 21.5\,T_{surf} - 1.27\,PAR - 10.6\,U$	0.306
7 days		
$T_{surf} + PAR + prec + U_w$	$545 + 37.9\,T_{surf} - 1.95\,PAR + 723\,prec - 87.8\,U_w$	0.516
$T_{surf} + PAR + U_w$	$563 + 38\,T_{surf} - 2.18\,PAR + 200\,U_w$	0.493
$T_{surf} + PAR + U_w + U$	$471 + 39\,T_{surf} - 2.12\,PAR + 245\,U_w + 28.3\,U$	0.452
$T_{surf} + PAR$	$686 + 31.6\,T_{surf} - 2.12\,PAR$	0.443
$T_{surf} + PAR + prec$	$674 + 28.7\,T_{surf} - 1.83\,PAR + 514\,prec$	0.433

300 itations during calm or moderate wind conditions (Spank et al., 2020), when the advection of gases from land also poses a problem for the EC flux measurements, not representing the surface gas exchange in these cases.

Standard low turbulence filtering criteria based on friction velocity or standard deviation of vertical component of wind velocity are not recommended for EC fluxes over lakes and rivers, as the wind shear generated turbulence is one of the main driver of gas exchange at water-air interface. Here, we have proposed the method of dividing the 30-minute intervals into shorter

305 5-minute sub-intervals, which reveals how short term changes in wind directions may contaminate the measured CO_2 signal, affecting the quality of measured 30-minutes fluxes (Fig. A2). Removing these situations when the flux signal originates from land makes the measured flux closer to an unbiased estimate of the gas exchange between the water surface and the atmosphere.

Few different approaches have been proposed for filtering low turbulence and/or advection dominated conditions, based on e.g. a minimum threshold value for the atmospheric stability (Czikowsky et al., 2018) or a maximum threshold for the standard

310 deviation of atmospheric CO_2 mixing ratio (Erkkilä et al., 2018). The choice of threshold values is a mostly empirical, partly arbitrary and often site-specific choice for e.g. stability, friction velocity or gas mixing ratio. Despite our new wind sub-interval filtering method, we still had to implement a screening based on maximum threshold values of standard deviation of gas mixing ratios. This demonstrates the challenges in and importance of finding the correct criteria for the data screening.

Table 5. Multivariate linear regression models between CO_2 fluxes and surface temperature (T_{surf}, [°C]), partial pressure of CO_2 in water (pCO_{2w}, [µatm]), photosynthetically active radiation (PAR, [µmol m^{-2} s^{-1}]), wind speed (U, [m s^{-1}]), precipitation (prec, [mm d^{-1}]) and water flow speed (U_w, [m s^{-1}]) that give the highest value of R^2_{adj} at time scales (averaging periods) of 24 hours and 7 days. The Wilkinson notation is used in describing the combination of the variables. In the model formula, the unit of the intersection is µmol m^{-2} s^{-1} and the units of the variables' multipliers are µmol m^{-2} s^{-1}/[unit of variable]. Only statistically significant models are shown.

Combination	Formula	R^2_{adj}
24 h		
$pCO_{2w} + PAR + U_w + U$	$-0.485 + 0.000664\,pCO_{2w} - 0.000367\,PAR + 0.502\,U_w + 0.092\,U$	0.621
$pCO_{2w} + PAR + prec + U_w + U$	$-0.484 + 0.000661\,pCO_{2w} - 0.000348\,PAR + 0.0254\,prec + 0.492\,U_w + 0.092\,U$	0.613
$T_{surf} + pCO_{2w} + PAR + U_w + U$	$-0.488 + 0.000938\,T_{surf} + 0.000655\,pCO_{2w} - 0.000394\,PAR + 0.495\,U_w + 0.0925\,U$	0.613
$pCO_{2w} + U_w + U$	$-0.599 + 0.000724\,pCO_{2w} + 0.405\,U_w + 0.103\,U$	0.610
$T_{surf} + pCO_{2w} + U_w + U$	$-0.537 - 0.00502\,T_{surf} + 0.000752\,pCO_{2w} + 0.483\,U_w + 0.0955\,U$	0.609
7 days		
$T_{surf} + pCO_{2w} + prec + U_w + U$	$-0.533 - 0.0486\,T_{surf} + 0.000476\,pCO_{2w} - 2.94\,prec + 8.91\,U_w + 0.0528\,U$	0.928
$T_{surf} + pCO_{2w} + prec + U_w$	$-0.385 - 0.0565\,T_{surf} + 0.000441\,pCO_{2w} - 3.21\,prec + 9.91\,U_w$	0.919
$T_{surf} + pCO_{2w} + PAR + prec + U_w$	$-0.253 - 0.0421\,T_{surf} + 0.000315\,pCO_{2w} - 0.000676\,PAR - 2.62\,prec + 8.57\,U_w$	0.913
$pCO_{2w} + PAR + prec + U_w + U$	$-0.244 + 0.000191\,pCO_{2w} - 0.00174\,PAR - 0.771\,prec + 3.67\,U_w + 0.0773\,U$	0.868
$pCO_{2w} + PAR + U_w + U$	$-0.153 + 0.000203\,pCO_{2w} - 0.00157\,PAR + 2.63\,U_w + 0.0679\,U$	0.861

4.2 Magnitude and temporal dynamics of fluxes

315 So far, only Huotari et al. (2013) have reported EC CO_2 fluxes over a river. Measurements have been carried out for about one month in summer 2009 at the River Kymijoki (southern Finland), which is wider than River Kitinen and has a mean annual discharge 2.7 times as large as that of Kitinen, resulting in higher water flow velocity ranging between 0.15 and 1.17 m s^{-1}, with a mean value of 0.66 m s^{-1} (Huotari et al., 2013). The mean F_{CO_2} over Kymijoki during their measurements was 0.94 ± 0.5 µmol m^{-2} s^{-1}, 2.5 times as high as F_{CO_2} over Kitinen during the KITEX campaign. Huotari et al. (2013) attributed changes

320 in the measured flux to changes in pCO_2 in the water, which in turn was negatively correlated with discharge. Contrary to this study, Huotari et al. (2013) did not detect any significant diurnal cycle in F_{CO_2}. They measured pCO_2 to be approximately 600–1000 µatm, which is less than what was measured during the KITEX campaign. The larger F_{CO_2} in Kymijoki is then likely due to the larger water flow velocity, enhancing the efficiency of gas exchange at the air-water interface.

Diurnal changes in pCO_2 in a boreal lake have been linked with photosynthetic activity and ecosystem respiration in the

325 water (Åberg et al., 2010) and that is likely the case in a boreal river as well. Although subsaturation of dissolved CO_2 relative to the atmosphere was not detected at the Kitinen platform, it is still possible that lateral gradients exist in the pCO_{2w} due to higher photosynthesis close to the river banks, and that during the day, some parts of the river could be subsequently subsaturated with CO_2. The negative correlation found between pCO_{2w} and PAR in River Kitinen supports this hypothesis.

Table 6. Multivariate linear regression models between CH_4 fluxes and surface temperature (T_{surf}, [°C]), partial pressure of CO_2 in water (pCO_{2w}, [µatm]), photosynthetically active radiation (PAR, [µmol m^{-2} s^{-1}]), wind speed (U, [m s^{-1}]), precipitation (prec, [mm d^{-1}]) and water flow speed (U_w, [m s^{-1}]) that give the highest value of R^2_{adj} at time scales (averaging periods) of 24 hours and 7 days. The Wilkinson notation is used in describing the combination of the variables. In the model formula, the unit of the intersection is nmol m^{-2} s^{-1} and the units of the variables' multipliers are nmol m^{-2} s^{-1}/[unit of variable]. Only statistically significant models are shown.

Combination	Formula	R^2_{adj}
24 h		
$T_{surf} + U$	$-0.211 + 0.157\,T_{surf} + 0.599\,U$	0.220
$T_{surf} + PAR + U$	$-0.2 + 0.17\,T_{surf} - 0.00126\,PAR + 0.58\,U$	0.206
$T_{surf} + prec + U$	$-0.21 + 0.157\,T_{surf} - 0.0261\,prec + 0.599\,U$	0.204
$T_{surf} + U_w + U$	$-1.72 + 0.186\,T_{surf} + 7.01\,U_w + 0.634\,U$	0.201
$T_{surf} + PAR + prec + U$	$-0.17 + 0.171\,T_{surf} - 0.00151\,PAR - 0.402\,prec + 0.582\,U$	0.189
7 days		
$T_{surf} + PAR + U_w + U$	$1.15 + 0.408\,T_{surf} - 0.0162\,PAR - 17.1\,U_w + 0.507\,U$	0.875
$T_{surf} + PAR + U_w$	$2.81 + 0.393\,T_{surf} - 0.0178\,PAR - 17.8\,U_w$	0.792
$T_{surf} + pCO_{2w} + PAR$	$3.03 + 0.28\,T_{surf} - 0.00165\,pCO_{2w} - 0.0141\,PAR$	0.766
$T_{surf} + pCO_{2w} + U$	$-3.28 + 0.199\,T_{surf} + 0.00392\,pCO_{2w} + 0.514\,U$	0.759
$T_{surf} + PAR + U$	$0.304 + 0.292\,T_{surf} - 0.0119\,PAR + 0.376\,U$	0.751

Some earlier studies on boreal and arctic rivers have reported CO_2 fluxes measured by floating chambers. Although they represent different spatial and temporal scales, the mean values of such fluxes can still be compared to the magnitude of EC fluxes from our study. Huttunen et al. (2002) carried out chamber measurements at the hydroelectric reservoir Porttipahta, which is 75 km upstream of the KITEX experiment site. The measurements were conducted in 1995 when the reservoir had existed for 28 years. They detected fluxes which were relatively close (within 50 %–150 %) to our observations, the mean F_{CO_2} being 0.57 µmol m^{-2} s^{-1}. Silvennoinen et al. (2008) measured a mean CO_2 flux of 5.2 µmol m^{-2} s^{-1} from the small, eutrophic River Temmesjoki in central Finland during summer. The mean F_{CO_2} from the River Kolyma main stem in eastern Siberia was 0.5 µmol m^{-2} s^{-1}, relatively close to that of Kitinen (Denfeld et al., 2013). Campeau et al. (2014) determined F_{CO_2} from boreal streams and rivers (Strahler orders 1–6) in Quebec in Canada to be 0.85 µmol m^{-2} s^{-1}. Other studies have revealed substantially larger emissions of CO_2, such as 2.0 µmol m^{-2} s^{-1} on River Yukon in Alaska (Striegl et al., 2012) and 6.2 µmol m^{-2} s^{-1} on different-sized western Siberian river systems in Russia during summer (6.3 µmol m^{-2} s^{-1} if only areas without permafrost are considered) (Serikova et al., 2018). None of these studies focused on diurnal differences in the emissions.

Recently, differences in the day- and nighttime F_{CO_2} over rivers have been observed globally (Gómez-Gener et al., 2021) and in European streams and small rivers (Attermeyer et al., 2021). Floating chamber measurements may be biased towards daytime measurements. In this aspect, EC measurements fill the need for continuous measurements with higher temporal

345   resolution. Indeed, our findings show that sampling only during the day would give a considerably underestimated value of F_{CO_2} and a slight overestimation of F_{CH_4}, the average daytime fluxes being 220 % and 80 % of the nighttime fluxes for CO_2 and CH_4, respectively. Continuous sampling is therefore recommended for unbiased averaged flux estimates.

Both Gómez-Gener et al. (2021) and Attermeyer et al. (2021) found that the day-night difference in fluxes was mainly driven by a diurnal change in water-side pCO_2, which results from daytime photosynthetic fixation of CO_2. The day-night difference

350   in F_{CO_2} observed by Attermeyer et al. (2021) using drifting chambers was on average 0.14 μmol m^{-2} s^{-1}. Our study showed a considerably larger difference, potentially suggesting a difference in streams and rivers as gas emittors. This difference could be related to changes in pCO_2, following the result by Rocher-Ros et al. (2019) that the magnitude of gas evasion is controlled by the supply of the said gas in the river.

No earlier studies on CH_4 emissions from rivers have been previously conducted with EC. Consequently, comparison to

355   similar studies cannot be done. Still, CH_4 emissions from boreal rivers have been measured with floating chambers. Huttunen et al. (2002) measured F_{CH_4} to be 2.6 nmol m^{-2} s^{-1} from the boreal reservoir Porttipahta, which is very close to the mean value of 3.9 nmol m^{-2} s^{-1} measured during this field campaign. Silvennoinen et al. (2008) reported a larger emission of F_{CH_4} of 63 nmol m^{-2} s^{-1} from the Estuary of Temmesjoki River in the shallow Liminganlahti Bay in Finland. Other earlier studies report similar CH_4 flux magnitude (94 nmol m^{-2} s^{-1}) as averaged value from different stream orders and seasons in two

360   boreal regions in Quebec, Canada (Campeau et al., 2014).

Sieczko et al. (2020) show that methane emissions from lakes can indeed have a diel cycle and that the higher daytime emissions are likely caused by a higher wind speed and the occurrence of ebullition. In our study, there were no significant differences between daytime and nighttime F_{CH_4}, but we found higher daily and weekly mean flux in July when we recorded the highest values of PAR and water temperature. Similarly, Rovelli et al. (2021) found no diurnal difference in CH_4 emissions

365   from a river which they attribute to mixing in the river.

4.3   Drivers of pCO_{2w} and fluxes

Although many of the previous studies have been conducted in streams, i.e. with a lower Strahler order, it is likely that the same processes that drive the flux apply in rivers as well but with a different relative importance (Hotchkiss et al., 2015). The models that contain pCO_{2w} explain a large part of the variability in F_{CO_2}, similarly to what has been found in other rivers

370   (e.g., Rocher-Ros et al., 2020).

The source of CO_2 in the river can be the soil catchment, where the CO_2 is flushed as either dissolved organic or inorganic carbon or directly injected as CO_2 (Hotchkiss et al., 2015), or it can be the result of aquatic ecosystem metabolism taking place in the river itself (Hall et al., 2016). pCO_{2w} in Kitinen was controlled mainly by T_{surf} and PAR with a positive and negative response, respectively. They are the drivers of the net ecosystem exchange which consists of the assimilation of CO_2

375   by photosynthesis and release of CO_2 by respiration. The uptake of CO_2 in a river is controlled by available light and the amount of respiration by temperature (Lynch et al., 2010). Temperature also affects the composition of dissolved inorganic carbon in the river (Spank et al., 2020) and changes the CO_2 solubility (Chien et al., 2018). Terrestrial photosynthesis and respiration potentially act at different temporal scales than in the river, in addition to which the runoff-induced time delay

further complicates the comparison between pCO_{2w} and terrestrial cycles. Still, the dependence of CO_2 on both T and PAR is
380   evident on both daily and weekly timescales which suggests that processes taking place at both time scales could be important.
Precipitation is the key factor in runoff, however, the measured precipitation at one point might not be completely representative
of the total precipitation over the entire watershed. Nevertheless, the precipitation appears in some models for pCO_{2w}, likely
indicating that both local and terrestrial sources of CO_2 affect pCO_{2w} in Kitinen, but their relative contribution is unknown.

The response of pCO_{2w} to U_w was positive on both daily and weekly timescales. Liu and Raymond (2018) found a negative
385   correlation between pCO_{2w} and discharge in stream order up to 4 and no correlation in streams of order 5. Campeau and
del Giorgio (2014) found a negative correlation between U_w and pCO_{2w}, using data from stream orders 1–6. Small rivers are
more prone to evade than transport gases in which case the correlation is negative as higher flow velocities enhance mixing in
the river (Liu and Raymond, 2018). Positive correlation implies an added advection of CO_2 in the river and possibly added
flushing of soils. As a middle-sized river, the River Kitinen falls in the intermediate range where the relative importance of
390   U_w on the gas dynamics is smaller than in small rivers (Alin et al., 2011). This is supported also by Guseva et al. (2021),
who found that bottom-generated turbulence was the dominant factor in controlling near-surface turbulence during 40% of
the time during the KITEX campaign. This result also implies that in mid-sized or large controlled rivers, controlling of the
flow velocity accounts to a significant part of the changes in pCO_{2w}. Note also that the correlation of pCO_{2w} and U_w on daily
and weekly timescales reveals a more complex picture of their correlation than just coincidental matching of daily variability,
395   caused by biology (pCO_{2w}) and dam operations (U_w).

Contrary to U_w, the response of pCO_{2w} to U was negative in the best daily models. Still, it occurred as a driver in only some
of the best models. Scofield et al. (2016) found a negative correlation between pCO_{2w} and wind speed in the large River Negro
in Amazon which they attribute to the importance of the wind speed controlling the outgassing. However, our results indicate
that the significance of U as a driver of pCO_{2w} in Kitinen is limited as it appears in only some of the best daily models. The two
400   variables can also exhibit intercorrelation but not necessarily causality. For example, high daily wind speeds coincided with
low daily pCO_{2w} values during early summer and late autumn but were caused by different factors: atmospheric dynamics vs.
high dilution by precipitation and low respiration due to low water temperature.

It is evident from Table 5 that the main driver of CO_2 fluxes in our study are pCO_{2w}, U_w and U, both on daily and weekly
timescales. The dependence on pCO_{2w} is expected and has been shown in many earlier studies (e.g., Hutchins et al., 2020).
405   Although the drivers of diel cycles were not tested, these are the drivers that also control the metabolism in rivers (Rocher-Ros
et al., 2020) and the related diurnal pattern in CO_2 fluxes observed in our dataset.

Liu and Raymond (2018) showed in their study a dependence of F_{CO_2} on the discharge and thus U_w, which can be explained
by either U_w directly increasing mixing in the river by means of bottom friction (Liu et al., 2017), or by flushing of surrounding
soils. As U_w appears more in daily than weekly models and the flushing is a slower process than mixing in the river, it is likely
410   the enhanced mixing that contributes to the regression. However, as the daily control cycle of the discharge is so pronounced,
the temporal correlation could also explain part of the observed correlation. Precipitation works similarly as U_w that it enhances
mixing in the river, particularly the surface water, and increases the runoff in the watershed. On the other hand, the locally-

observed precipitation does not incorporate all of the precipitation events over the watershed and thus precipitation is not highly important as a driver.

415   U is known to control the efficiency of air-water gas exchange by means of surface shear generated turbulence in lakes and ocean, and it has been observed in earlier studies to be an important factor also over large rivers (e.g., Alin et al., 2011; Hall and Ulseth, 2019). Our results show U to be a significant driver of F_{CO_2} both at the daily and weekly scales.

For lakes, the CH_4 production in sediments depends exponentially on the sediment temperature beside the O_2 and CO_2 concentrations (e.g. Stepanenko et al., 2016). Produced CH_4 is then transported towards the surface by diffusion and turbulence being prone to oxidation, which depends on the O_2 concentration in the water column. Some fraction of CH_4 flux may evolve by ebullition avoiding oxidation. It was not tried to identify ebullition in the EC data. However, the overall magnitude of CH_4 fluxes was low which does not support the possibility of ebullition.

Water temperature is the most important driver of CH_4 emissions (Yvon-Durocher et al., 2014; Stanley et al., 2016) and it is clearly visible also in all best models (Table 6). In addition, the wind speed can have a quick physical forcing on either water-column processes (vertical mixing) or directly on the surface flux (gas transfer coefficient) and thus it appears as the important driver also at the daily and weekly scale.

Rovelli et al. (2021) describes CH_4 dynamics for small streams by following: CH_4 shows a nonlinear response to seasonal changes in discharge and is predominantly produced in the stream bed. Once released from the bed, outgassing of CH_4 at the surface and flow-driven dilution occur far more rapidly than biological methane oxidation. In lakes, CH_4 is likewise borne from biological processes in the sediment and then transported mostly vertically (e.g. Stepanenko et al., 2016). As a regulated river, the characteristics of River Kitinen are between small streams and lakes. Although $p_{CH_4,w}$ and sediment temperature were not measured during the campaign nor were all the drivers of CH_4 production, consumption, anaerobic metabolism and ecosystem energetics (like quality of organic matter, nutrients; see Stanley et al. (2016)), the multivariate regression analysis reveals the combined biotic and abiotic features of CH_4 flux drivers. The results described above corroborate the general picture of CH_4 production and transport.

Campeau and del Giorgio (2014) and Hutchins et al. (2019) found a positive correlation between $p_{CO_2,w}$ and $p_{CH_4,w}$ in streams and rivers in boreal Canada. As we did not measure $p_{CH_4,w}$, we cannot analyse this correlation in River Kitinen, but we included $p_{CO_2,w}$ as a variable in the multivariate analysis. It appears as a driver in some of the weekly models but with a variable sign in response. This ambiguity can be explained simply by the overall weak indirect linkage between $p_{CO_2,w}$, $p_{CH_4,w}$ and the CH_4 flux. Still, the positive correlation with T_{surf} and negative with PAR, the most significant drivers of $p_{CO_2,w}$, could suggest a linkage between $p_{CO_2,w}$ and $p_{CH_4,w}$.

Finally, we found a negative correlation between PAR and F_{CH_4}. The correlation at the daily scale is weak as PAR exists as a variable in only some models. Additionally, while the magnitude of F_{CH_4} was at its highest in late July and early August, PAR peaked in early July which, in turn, reduces the daily correlation. PAR and CH_4 flux have been found to correlate positively in stratified lakes due to photosynthesis-driven oxic methane production (Günthel et al., 2020) and light-dependent aerobic methane oxidation (Oswald et al., 2015). These processes are therefore likely non-important in River Kitinen.

5 Conclusions

In this study, we have reported results from a four months field campaign over a boreal river, including the longest CO_2 and the first ever CH_4 continuous flux data measured on a river by using the eddy covariance method. On average, the river was a net source of CO_2 and CH_4 to the atmosphere. The CO_2 fluxes shown clear seasonal variation, reaching the maximum monthly value of $0.44 \pm 0.32 \mu mol m^{-2} s^{-1}$ in August, and the minimum of 0.19 ± 0.31 µmol m^{-2} s^{-1} in June. We found a statistically significant difference ($p < 0.05$) between the daytime and nighttime fluxes during June, July and August of 0.48, 0.39 and 0.48 µmol m^{-2} s^{-1}, respectively. In addition, we found that the main physical drivers of $p_{CO_2,w}$ were T_{surf} and PAR. The CO_2 fluxes were mainly driven by $p_{CO_2,w}$ and PAR while the main drivers for CH_4 fluxes were T_{surf} and U. Similar additional studies in rivers are needed as the EC observations complement chamber observations providing information at the ecosystem scale but with a better temporal resolution. As rivers represent spatially small ecosystems with limited fetches, special care is required in the source area analysis by footprint modelling and filtering out the contribution from the land. This is a prerequisite for the accurate detection of e.g. diurnal cycles in fluxes. The more detailed observation of the wind direction fluctuations has appeared to be an effective tool for identifying and removing of EC data affected by air masses coming from the nearby shore.

Due to the controlled nature of the River Kitinen, it does not necessarily represent a river in a natural state. Nonetheless, as most of the world's rivers are dammed, the response of fluxes and the dissolved CO_2 partial pressure on the discharge could provide valuable insight into gas emissions from controlled rivers.

Data availability. Data are available upon request from the corresponding author.

Author contributions. TV, ALi, ALo, SM and IM designed the field experiments. AV, SG, ALi, ALo and SM carried out the field measurements. ALi measured the pCO_2 in air and water. AV and IM conducted the eddy covariance data processing and analysis. AV, TV and IM prepared the manuscript with contribution from all coauthors.

Competing interests. The authors declare no competing interests.

Acknowledgements. AV, IM and TV acknowledge financial support from Research Council of Finland (ICOS-FIRI and Project 322432), ICOS-FI via University of Helsinki funding, the EU Horizon Europe Framework Programme for Research and Innovation (GreenFeedback nr. 101056921). ALo acknowledges funding through the German Research Foundation (Grant no. LO1150/12). Finally, we would like to thank the technical staff at the Arctic Space Centre of Finnish Meteorological Institute in Sodankylä for the technical support.

References

Åberg, J., Jansson, M., and Jonsson, A.: Importance of water temperature and thermal stratification dynamics for temporal variation of surface water CO_2 in a boreal lake, J. Geophys. Res., 115, G02 024, https://doi.org/10.1029/2009JG001085, 2010.

475 Alin, S. R., de Fátima F.L. Rasera, M., Salimon, C. I., Richey, J. E., Holtgrieve, G. W., Krusche, A. V., and Snidvongs, A.: Physical controls on carbon dioxide transfer velocity and flux in low-gradient river systems and implications for regional carbon budgets, J. Geophys. Res., 116, G01 009, https://doi.org/10.1029/2010JG001398, 2011.

Attermeyer, K., Casas-Ruiz, J. P., Fuss, T., Pastor, A., Cauvy-Fraunié, S., Sheath, D., Nydahl, A. C., Doretto, A., Portela, A. P., Doyle, B. C., Simov, N., Gutmann Roberts, C., Niedrist, G. H., Timoner, X., Evtimova, V., Barral-Fraga, L., Bašić, T., Audet, J., Deininger, A.,

480 Busst, G., Fenoglio, S., Catalán, N., de Eyto, E., Pilotto, F., Mor, J.-R., Monteiro, J., Fletcher, D., Noss, C., Colls, M., Nagler, M., Liu, L., González-Quijano, C. R., Romero, F., Pansch, N., Ledesma, J. L. J., Pegg, J., Klaus, M., Freixa, A., Herrero Ortega, S., Mendoza-Lera, C., Bednařík, A., Fonvielle, J. A., Gilbert, P. J., Kenderov, L. A., Rulík, M., and Bodmer, P.: Carbon dioxide fluxes increase from day to night across European streams, Commun. Earth Environ., 2, 1–8, https://doi.org/10.1038/s43247-021-00192-w, 2021.

Aubinet, M., Grelle, A., Ibrom, A., Rannik, Ü., Moncrieff, J., Foken, T., Kowalski, A. S., Martin, P. H., Berbigier, P., Bernhofer, C., Clement,

485 R., Elbers, J., Granier, A., Grunwald, T., Morgenstern, K., Pilegaard, K., Rebmann, C., Snijders, W., Valentini, R., and Vesala, T.: Estimates of the annual net carbon and water exchange of forests: The EUROFLUX methodology, Adv. Ecol. Res., 30, 113–175, 2000.

Aufdenkampe, A. K., Mayorga, E., Raymond, P. A., Melack, J. M., Doney, S. C., Alin, S. R., Aalto, R. E., and Yoo, K.: Riverine coupling of biogeochemical cycles between land, oceans, and atmosphere, Front. Ecol. Environ., 9, 53–60, https://doi.org/10.1890/100014, 2011.

Baldocchi, D. D.: Assessing the eddy covariance technique for evaluating carbon dioxide exchange rates of ecosystems: past, present and

490 future, Glob. Change Biol., 9, 479–492, 2003.

Bastviken, D., Sundgren, I., Natchimuthu, S., Reyier, H., and Gålfalk, M.: Technical Note: Cost-efficient approaches to measure carbon dioxide (CO_2) fluxes and concentrations in terrestrial and aquatic environments using mini loggers, Biogeosciences, 12, 3849–3859, https://doi.org/10.5194/bg-12-3849-2015, 2015.

Burba, G., Schmidt, A., Scott, R. L., Nakai, T., Kathilankal, J., Fratini, G., Hanson, C., Law, B., McDermitt, D. K., Eckles, R., Furtaw, M.,

495 and Velgersdyk, M.: Calculating CO_2 and H_2O eddy covariance fluxes from an enclosed gas analyzer using an instantaneous mixing ratio, Glob. Change Biol., 18, 385–399, https://doi.org/10.1111/j.1365-2486.2011.02536.x, 2012.

Campeau, A. and del Giorgio, P. A.: Patterns in CH_4 and CO_2 concentrations across boreal rivers: Major drivers and implications for fluvial greenhouse emissions under climate change scenarios, Glob. Change Biol., 20, 1075–1088, https://doi.org/10.1111/gcb.12479, 2014.

Campeau, A., Lapierre, J.-F., Vachon, D., and del Giorgio, P. A.: Regional contribution of CO_2 and CH_4 fluxes from the fluvial network in

500 a lowland boreal landscape of Québec, Global Biogeochemical Cy., 28, 57–69, https://doi.org/10.1002/2013GB004685, 2014.

Chen, H., Winderlich, J., Gerbig, C., Hoefer, A., Rella, C. W., Crosson, E. R., Van Pelt, A. D., Steinbach, J., Kolle, O., Beck, V., Daube, B. C., Gottlieb, E. W., Chow, V. Y., Santoni, G. W., and Wofsy, S. C.: High-accuracy continuous airborne measurements of greenhouse gases (CO_2 and CH_4) using the cavity ring-down spectroscopy (CRDS) technique, Atmos. Meas. Tech., 3, 375–386, 2010.

Chien, H., Zhong, Y.-Z., Yang, K.-H., and Cheng, Hao, Y.: Diurnal variability of CO_2 flux at coastal zone of Taiwan based of eddy covariance

505 observations, Cont. Shelf Res., 162, 27–38, https://doi.org/10.1016/j.csr.2018.04.006, 2018.

Cole, J. J., Prairie, Y. T., Caraco, N. F., McDowell, W. H., Tranvik, L. J., Striegl, R. G., Duarte, C. M., Kortelainen, P., Downing, J. A., Middelburg, J. J., and Melack, J.: Plumbing the global carbon cycle: integrating inland waters into the terrestrial carbon budget, Ecosystems, 10, 171–184, https://doi.org/10.1007/s10021-006-9013-8, 2007.

Czikowsky, M. J., MacIntyre, S., Tedford, E. W., Vidal, J., and Miller, S. D.: Effects of wind and buoyancy on carbon dioxide distribution
510   and air-water flux of a stratified temperate lake, J. Geophys. Res.-Biogeo., 123, 2305–2322, https://doi.org/10.1029/2017JG004209, 2018.

Denfeld, B. A., Frey, K. E., Sobczak, W. V., Mann, P. J., and Holmes, R. M.: Summer CO_2 evasion from streams and rivers in the Kolyma
       River basin, north-east Siberia, Polar Res., 32, 19 704, https://doi.org/10.3402/polar.v32i0.19704, 2013.

Drake, T. W., Raymond, P. A., and Spencer, R. G. M.: Terrestrial carbon inputs to inland waters: A current synthesis of estimates and
       uncertainty, Limnol. Oceanogr. Letters, 3, 132–142, https://doi.org/10.1002/lol2.10055, 2018.

515   Erkkilä, K.-M., Ojala, A., Bastviken, D., Biermann, T., Heiskanen, J. J., Lindroth, A., Peltola, O., Rantakari, M., Vesala, T., and Mammarella,
       I.: Methane and carbon dioxide fluxes over a lake: comparison between eddy covariance, floating chambers and boundary layer method,
       Biogeosciences, 15, 429–445, https://doi.org/10.5194/bg-15-429-2018, 2018.

Eugster, W., DelSontro, T., Shaver, G. R., and Kling, G. W.: Interannual, summer, and diel variability of CH_4 and CO_2 effluxes from Toolik
       Lake, Alaska, during the ice-free periods 2010–2015, Environ. Sci.-Proc. Imp., 22, 2181–2198, https://doi.org/10.1039/D0EM00125B,
520   2020.

Foken, T. and Wichura, B.: Tools for quality assessment of surface-based flux measurements, Agr. Forest Meteorol., 78, 83–105, 1996.

Golub, M., Koupaei-Abyazani, N., Vesala, T., Mammarella, I., Ojala, A., Bohrer, G., Weyhenmeyer, G. A., Blanken, P. D., Eugster, W.,
       Koebsch, F., Chen, J., Czajkowski, K., Deshmukh, C., Guerin, F., Heiskanen, J., Humphreys, E., Jonsson, A., Karlsson, J., Kling, G., Lee,
       X., Liu, H., Lohila, A., Lundin, E., Morin, T., Podgrajsek, E., Provenzale, M., Rutgersson, A., Sachs, T., Sahlee, E., Serca, D., Shao, C.,
525   Spence, C., Strachan, I. B., Xiao, W., and Desai, A. R.: Diel, seasonal, and inter-annual variation in carbon dioxide effluxes from lakes
       and reservoirs, Environ. Res. Lett., 18, https://doi.org/10.1088/1748-9326/acfb97, 2023.

Gómez-Gener, L., Rocher-Ros, G., Battin, T., Cohen, M. J., Dalmagro, H. J., Dinsmore, K. J., Drake, T. W., Duvert, C., Enrich-Prast, A.,
       Horgby, Å., Johnson, M. S., Kirk, L., Machado-Silva, F., Marzolf, N. S., McDowell, M. J., McDowell, W. H., Miettinen, H., Ojala,
       A. K., Peter, H., Pumpanen, J., Ran, L., Riveros-Iregui, D. A., Santos, I. R., Six, J., Stanley, E. H., Wallin, M. B., White, S. A.,
530   and Sponseller, R. A.: Global carbon dioxide efflux from rivers enhanced by high nocturnal emissions, Nat. Geosci., 14, 289–294,
       https://doi.org/10.1038/s41561-021-00722-3, 2021.

Günthel, M., Klawonn, I., Woodhouse, J., Bižić, M., Ionescu, D., Ganzert, L., Kümmel, S., Nijenhuis, I., Zoccarato, L., Grossart, H.-P.,
       and Tang, K. W.: Photosynthesis-driven methane production in oxic lake water as an important contributor to methane emission, Limnol.
       Oceanogr., 65, 2853–2865, https://doi.org/10.1002/lno.11557, 2020.

535   Guseva, S., Aurela, M., Cortés, A., Kivi, R., Lotsari, E., MacIntyre, S., Mammarella, I., Ojala, A., Stepanenko, V., Uotila, P., Vähä, A.,
       Vesala, T., Wallin, M. B., and Lorke, A.: Variable physical drivers of near-surface turbulence in a regulated river, Water Resour. Res., 57,
       e2020WR027 939, https://doi.org/10.1029/2020WR027939, 2021.

Hall, R. O. and Ulseth, A. J.: Gas exchange in streams and rivers, WIREs Water, 7, e1391, https://doi.org/10.1002/wat2.1391, 2019.

Hall, R. O., Tank, J. L., Baker, M. A., Rosi-Marshall, E. J., and Hotchkiss, E. R.: Metabolism, gas exchange, and carbon spiraling in rivers,
540   Ecosystems, 19, 73–86, https://doi.org/10.1007/s10021-015-9918-1, 2016.

Hotchkiss, E., Hall Jr, R., Sponseller, R., Butman, D., Klaminder, J., Laudon, H., Rosvall, M., and Karlsson, J.: Sources of and processes
       controlling CO_2 emissions change with the size of streams and rivers, Nat. Geosci., 8, 696–699, https://doi.org/10.1038/ngeo2507, 2015.

Huotari, J., Haapanala, S., Pumpanen, J., Vesala, T., and Ojala, A.: Efficient gas exchange between a boreal river and the atmosphere,
       Geophys. Res. Lett., 40, 5683–5686, https://doi.org/10.1002/2013GL057705, 2013.

545   Hutchins, R. H. S., Prairie, Y. T., and del Giorgio, P. A.: Large-scale landscape drivers of CO_2, CH_4, DOC, and DIC in boreal river networks,
       Global Biogeochemical Cy., 33, 125–142, https://doi.org/10.1029/2018GB006106, 2019.

Hutchins, R. H. S., Casas-Ruiz, J. P., Prairie, Y. T., and del Giorgio, P. A.: Magnitude and drivers of integrated fluvial network greenhouse gas emissions across the boreal landscape in Québec, Water Res., 173, 115 556, https://doi.org/10.1016/j.watres.2020.115556, 2020.

Huttunen, J., Väisänen, T., Hellsten, S., Heikkinen, M., Nykänen, H., Jungner, H., Niskanen, A., Virtanen, M., Lindqvist, O., Nenonen, O., and Martikainen, P.: Fluxes of CH_4, CO_2, and N_2O in hydroelectric reservoirs Lokka and Porttipahta in the northern boreal zone in Finland, Global Biogeochemical Cy., 16, 1003, https://doi.org/10.1029/2000GB001316, 2002.

Kljun, N., Calanca, P., Rotach, M. W., and Schmid, H. P.: A simple two-dimensional parameterisation for Flux Footprint Prediction (FFP), Geosci. Model Dev., 8, 3695–3713, https://doi.org/10.5194/gmd-8-3695-2015, 2015.

Kohonen, K.-M., Kolari, P., Kooijmans, L. M. J., Chen, H., Seibt, U., Sun, W., , and Mammarella, I.: Towards standardized processing of eddy covariance flux measurements of carbonyl sulfide, Atmos. Meas. Tech., 13, 3957–3975, https://doi.org/10.5194/amt-13-3957-2020, 2020.

Kristensen, L., Mann, J., Oncley, S. P., and Wyngaard, J. C.: How close is close enough when measuring scalar fluxes with displaced sensors?, J. Atmos. Ocean. Tech., 14, 814–821, 1997.

Lauerwald, R., Laruelle, G. G., Hartmann, J., Ciais, P., and Regnier, P. A. G.: Spatial patterns in CO_2 evasion from the global river network, Global Biogeochemical Cy., 29, 534–554, https://doi.org/10.1002/2014GB004941, 2015.

Li, M., Peng, C., Zhang, K., Xu, L., Wang, J., Yang, Y., Li, P., Liu, Z., and He, N.: Headwater stream ecosystem: an important source of greenhouse gases to the atmosphere, Water Res., 190, 116 738, https://doi.org/10.1016/j.watres.2020.116738, 2021.

Liu, H., Peters, G., and Foken, T.: New equations for sonic temperature variance and buoyancy heat flux with an omnidirectional sonic anemometer, Bound.-Lay. Meteorol., 100, 459–468, 2001.

Liu, S. and Raymond, P. A.: Hydrologic controls on pCO_2 and CO_2 efflux in US streams and rivers, Limnol. Oceanogr. Letters, 3, 428–435, https://doi.org/10.1002/lol2.10095, 2018.

Liu, S., Lu, X. X., Xia, X., Yang, X., and Ran, L.: Hydrological and geomorphological control on CO_2 outgassing from low-gradient large rivers: An example of the Yangtze River system, J. Hydrol., 550, 26–41, https://doi.org/10.1016/j.jhydrol.2017.04.044, 2017.

Lorke, A., Bodmer, P., Noss, C., Alshboul, Z., Koschorreck, M., Somlai-Haase, C., Bastviken, D., Flury, S., McGinnis, D. F., Maeck, A., Müller, D., and Premke, K.: Technical note: drifting versus anchored flux chambers for measuring greenhouse gas emissions from running waters, Biogeosciences, 12, 7013–7024, https://doi.org/10.5194/bg-12-7013-2015, 2015.

Lynch, J. K., Beatty, C. M., Seidel, M. P., Jungst, L. J., and DeGrandpre, M. D.: Controls of riverine CO_2 over an annual cycle determined using direct, high temporal resolution pCO_2 measurements, J. Geophys. Res., 115, G03 016, https://doi.org/10.1029/2009JG001132, 2010.

Mammarella, I., Launiainen, S., Gronholm, T., Keronen, P., Pumpanen, J., Rannik, Ü., and Vesala, T.: Relative humidity effect on the high-frequency attenuation of water vapor flux measured by a closed-path eddy covariance system, J. Atmos. Ocean. Tech., 26, 1856–1866, https://doi.org/10.1175/2009JTECHA1179.1, 2009.

Mammarella, I., Nordbo, A., Rannik, Ü., Haapanala, S., Levula, J., Laakso, H., Ojala, A., Peltola, O., Heiskanen, J., Pumpanen, J., and Vesala, T.: Carbon dioxide and energy fluxes over a small boreal lake in Southern Finland, J. Geophys. Res.-Biogeo., 120, 1296–1314, https://doi.org/10.1002/2014JG002873, 2015.

Mammarella, I., Peltola, O., Nordbo, A., Järvi, L., and Rannik, Ü.: Quantifying the uncertainty of eddy covariance fluxes due to the use of different software packages and combinations of processing steps in two contrasting ecosystems, Atmos. Meas. Tech., 9, 4915–4933, https://doi.org/10.5194/amt-9-4915-2016, 2016.

Nemitz, E., Mammarella, I., Ibrom, A., Aurela, M., Burba, G., Dengel, S., Gielen, B., Grelle, A., Heinesch, B., Herbst, M., Hörtnagl, L., Klemedtsson, L., Lindroth, A., Lohila, A., McDermitt, D., Meier, P., Merbold, L., Nelson, D., Nicolini, G., Nilsson, M., Peltola, O., Rinne, J., and Zahniser, M.: Standardization of eddy covariance flux measurements of methane and nitrous oxide, Int. Agrophys., 32, 517–549, https://doi.org/10.1515/intag-2017-0042, 2018.

Oswald, K., Milucka, J., Brand, A., Littmann, S., Wehrli, B., Kuypers, M. M. M., and Schubert, C. J.: Light-dependent aerobic methane oxidation reduces methane emissions from seasonally stratified lakes, PLoS ONE, 10, e0132 574, https://doi.org/10.1371/journal.pone.0132574, 2015.

Rannik, Ü. and Vesala, T.: Autoregressive filtering versus linear detrending in estimation of fluxes by the eddy covariance method, Bound.-Lay. Meteorol., 91, 259–280, 1999.

Raymond, P. A., Hartmann, J., Lauerwald, R., Sobek, S., McDonald, C., Hoover, M., Butman, D., Striegl, R., Mayorga, E., Humborg, C., Kortelainen, P., Dürr, H., Meybeck, M., Ciais, P., and Guth, P.: Global carbon dioxide emissions from inland waters, Nature, 503, 355–359, https://doi.org/10.1038/nature12760, 2013.

Regnier, P., Friedlingstein, P., Ciais, P., Mackenzie, F. T., Gruber, N., Janssens, I. A., Laruelle, G. G., Lauerwald, R., Luyssaert, S., Andersson, A. J., Arndt, S., Arnosti, C., Borges, A. V., Dale, A. W., Gallego-Sala, A., Godderis, Y., Goossens, N., Hartmann, J., Heinze, C., Ilyina, T., Joos, F., LaRowe, D. E., Leifeld, J., Meysman, F. J. R., Munhoven, G., Raymond, P. A., Spahni, R., Suntharalingam, P., and Thullner, M.: Anthropogenic perturbation of the carbon fluxes from land to ocean, Nat. Geosci., 6, 597–607, https://doi.org/10.1038/ngeo1830, 2013.

Rocher-Ros, G., Sponseller, R. A., Lidberg, W., Mörth, C.-M., and Giesler, R.: Landscape process domains drive patterns of CO_2 evasion from river networks, Limnol. Oceanogr. Letters, 4, 87–95, https://doi.org/10.1002/lol2.10108, 2019.

Rocher-Ros, G., Sponseller, R. A., Bergström, A., Myrstener, M., and Giesler, R.: Stream metabolism controls diel patterns and evasion of CO_2 in Arctic streams, Glob. Change Biol., 26, 1400–1413, https://doi.org/10.1111/gcb.14895, 2020.

Rocher-Ros, G., Stanley, E. H., Loken, L. C., Casson, N. J., Raymond, P. A., Liu, S., Amatulli, G., and Sponseller, R. A.: Global methane emissions from rivers and streams, Nature, 621, 530–535, https://doi.org/10.1038/s41586-023-06344-6, 2023.

Rovelli, L., Olde, L. A., Heppell, C. M., Binley, A., Yvon-Durocher, G., Glud, R. N., and Trimmer, M.: Contrasting biophysical controls on carbon dioxide and methane outgassing from streams, J. Geophys. Res.-Biogeo., 127, e2021JG006 328, https://doi.org/10.1029/2021JG006328, 2021.

Sabbatini, S., Mammarella, I., Arriga, N., Fratini, G., A., G., Hörtnagl, L., Ibrom, A., Longdoz, B., Mauder, M., Merbold, L., Metzger, S., Montagnani, L., Pitacco, A., Rebmann, C., Sedlak, P., Sigut, L., Vitale, D., and Papale, D.: Eddy covariance raw data processing for CO_2 and energy flux calculation at ICOS ecosystem stations, Int. Agrophys., 32, 495–515, https://doi.org/10.1515/intag-2017-0043, 2018.

Scofield, V., Melack, J. M., Barbosa, P. M., Amaral, J. H. F., Forsberg, B. R., and Farjalla, V. F.: Carbon dioxide outgassing from Amazonian aquatic ecosystems in the Negro River basin, Biogeochemistry, 129, 77–91, https://doi.org/10.1007/s10533-016-0220-x, 2016.

Serikova, S., Pokrovsky, O. S., Ala-aho, P., Kazantsev, V., Kirpotin, S. N., Kopysov, S. G., Krickov, I. V., Laudon, H., Manasypov, R. M., Shirokova, L. S., Soulsby, C., Tetzlaff, D., and Karlsson, J.: High riverine CO_2 emissions at the permafrost boundary of Western Siberia, Nat. Geosci., 11, 825–829, https://doi.org/10.1038/s41561-018-0218-1, 2018.

Sieczko, A. K., Duc, N. T., Schenk, J., Pajala, G., Rudberg, D., Sawakuchi, H. O., and Bastviken, D.: Diel variability of methane emissions from lakes, P. Natl. Acad. Sci. USA, 117, 21 488–21 494, https://doi.org/10.1073/pnas.2006024117, 2020.

Silvennoinen, H., Liikanen, A., Rintala, J., and Martikainen, P. J.: Greenhouse gas fluxes from the eutrophic Temmesjoki River and its Estuary in the Liminganlahti Bay (the Baltic Sea), Biogeochemistry, 90, 193–208, https://doi.org/10.1007/s10533-008-9244-1, 2008.

Spank, U., Hehn, M., Keller, P., Koschorreck, M., and Bernhofer, C.: A Season of Eddy-covariance Fluxes Above an Extensive Water Body Based on Observations from a Floating Platform, Bound.-Lay. Meteorol., 174, 433–464, https://doi.org/10.1007/s10546-019-00490-z, 2020.

Stanley, E. H., Casson, N. J., Christel, S. T., Crawford, J. T., Loken, L. C., and Oliver, S. K.: The ecology of methane in streams and rivers: patterns, controls, and global significance, Ecol. Monogr., 86, 146–171, https://doi.org/10.1890/15-1027, 2016.

Stepanenko, V., Mammarella, I., Ojala, A., Miettinen, H., Lykosov, V., and Vesala, T.: LAKE 2.0: a model for temperature, methane, carbon dioxide and oxygen dynamics in lakes, Geosci. Model Dev., 9, 1977–2006, https://doi.org/10.5194/gmd-9-1977-2016, 2016.

Striegl, R. G., Dornblaser, M. M., McDonald, C. P., Rover, J. R., and Stets, E. G.: Carbon dioxide and methane emissions from the Yukon River system, Global Biogeochemical Cy., 26, GB0E05, https://doi.org/10.1029/2012GB004306, 2012.

Verpoorter, C., Kutser, T., Seekell, D. A., and Tranvik, L. J.: A global inventory of lakes basen on high-resolution satellite imagery, Geophys. Res. Lett., 41, 6396–6402, https://doi.org/10.1002/2014GL060641, 2014.

Vickers, D. and Mahrt, L.: Quality control and flux sampling problems for tower and aircraft data, J. Atmos. Ocean. Tech., 14, 512–526, 1997.

Yvon-Durocher, G., Allen, A. P., Bastviken, D., Conrad, R., Gudasz, C., St-Pierre, A., Thanh-Duc, N., and Del Giorgio, P. A.: Methane fluxes show consistent temperature dependence across microbial to ecosystem scales, Nature, 507, 488–491, https://doi.org/10.1038/nature13164, 2014.

Appendix A: Data screening based on the wind direction

Figure A1 shows an example of a case when the calculated wind direction was within the accepted sectors but most of the instantaneous wind was not. In this case, the bulk wind direction was $155°$. However, only during the intervals 23:30–23:35 and 23:45–23:50 the 5-minute bulk wind direction fell within the accepted sectors. The horizontal wind speed varied between 0 and 3 m s^{-1} and the vertical wind between -1 and 1 m s^{-1}. A sudden change in the wind direction occurred at 23:54 when the wind abruptly turned east, i.e. from the forest. This caused a sudden $2°C$ drop in the measured sonic temperature and an increase of approximately 30 ppm in the CO_2 mixing ratio. The effect on H_2O and CH_4 was not as pronounced. The 30-minute CO_2 flux was as high as 11 µmol m^{-2} s^{-1}, caused mainly by the sudden increase in the mixing ratio, but with the 5-minute wind direction screening, the flux was only 0.09 µmol m^{-2} s^{-1}.
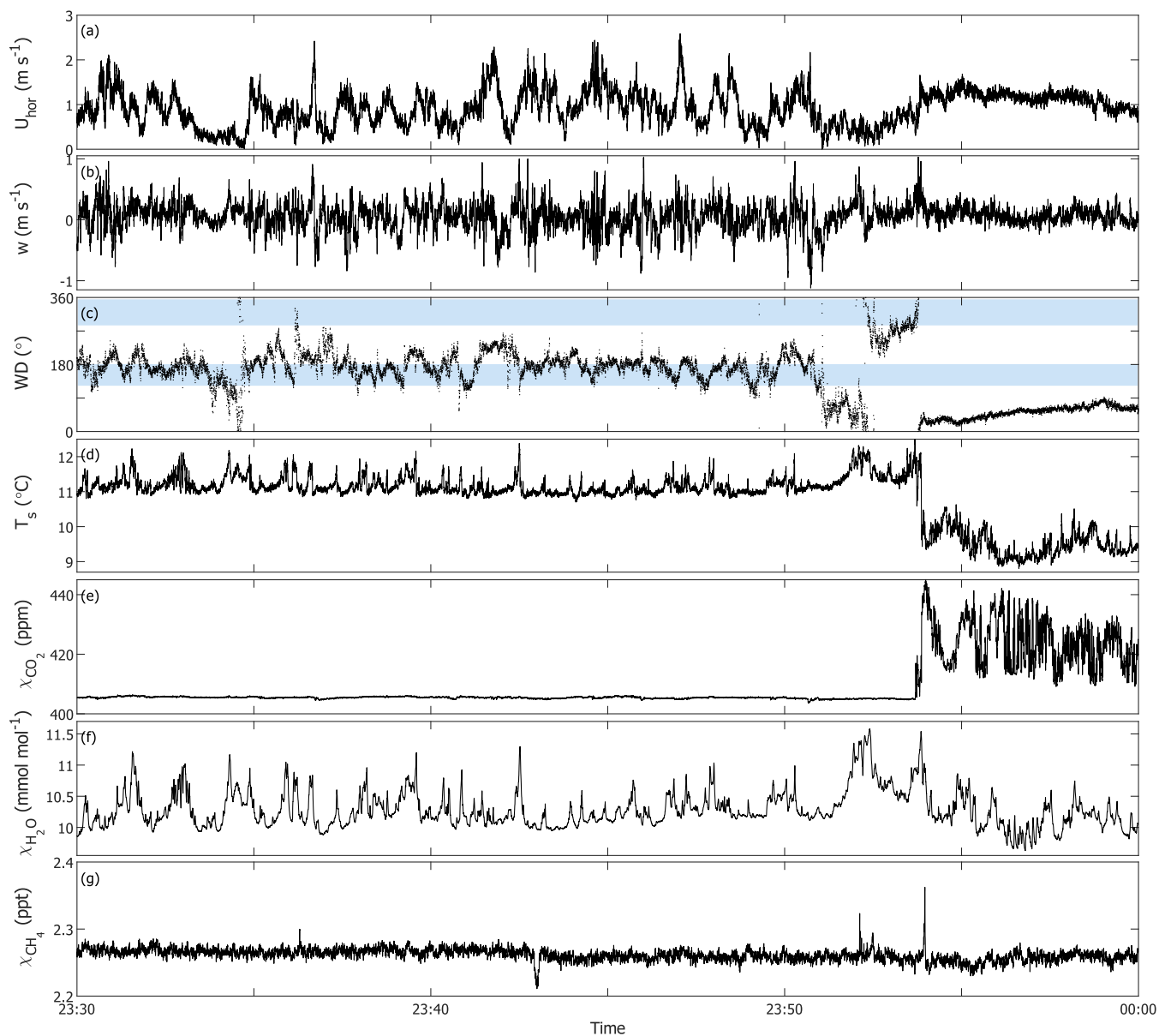
Figure A1. Example of a case with deviating wind direction on 7 August 2018 between 23:30 and 00:00 UTC. All data were measured at 10 Hz. (a) Horizontal wind speed. (b) Vertical wind speed. (c) Wind direction. The light-blue bars mark the accepted wind sectors. (d) Sonic temperature. (e) CO_2 dry mixing ratio. (f) H_2O mixing ratio. (g) CH_4 dry mixing ratio.
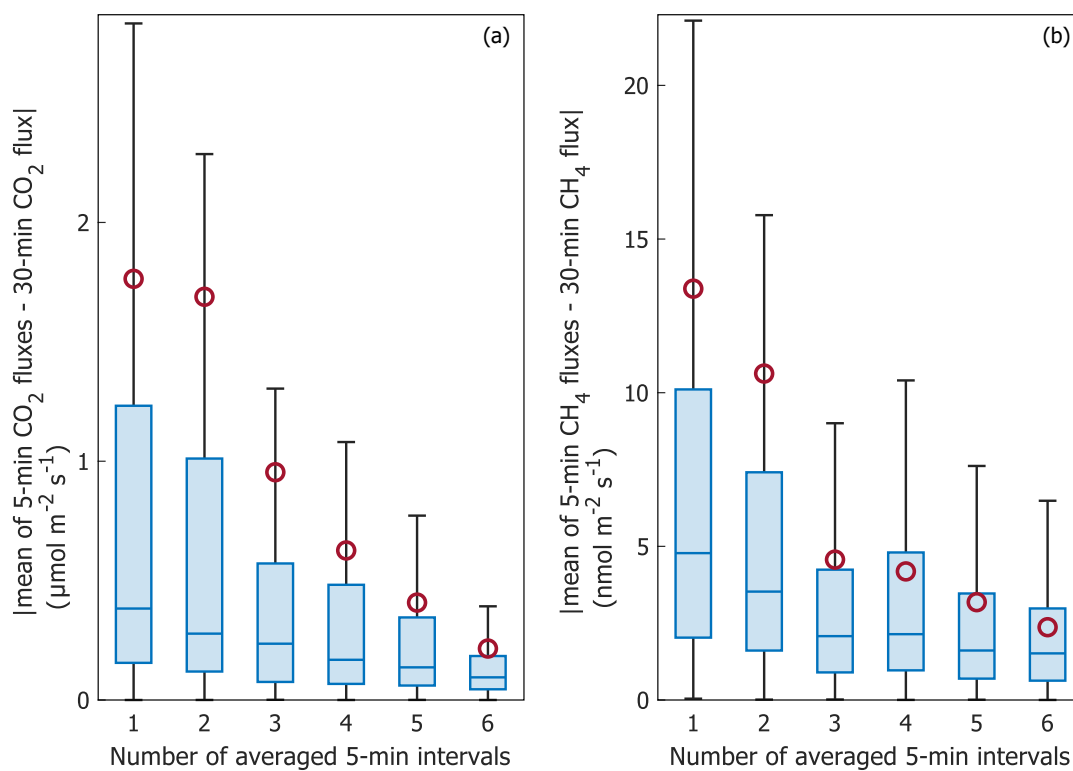
Figure A2. Absolute difference between the averaged 5 minutes and 30 minutes fluxes for CO_2 (a) and CH_4 (b) as a function of the number of averaged 5-minute intervals. The boxes indicate the upper and lower quartiles and the median. The whiskers are the maximum and minimum of nonoutliers. The circles indicate means. Outliers are not shown.